교육학 석사학위논문

Comparative study of electrochemical behavior of hydrogen peroxide using Prussian Blue analogues on poly(diallyldimethylammonium chloride) functionalized reduced Graphene oxide

환원 그래핀옥사이드-폴리(디알릴디메틸암모늄 클로라이드)과 니켈, 철, 구리 프러시안 블루의 합성과 과산화수소의 검출 비교 연구

2017년 2월

서울대학교 대학원
과학교육과 화학전공
오 효 재

CONTENT

List of Tables

List of Figures

Abstract

Comparative study of electrochemical behavior of hydrogen peroxide using Prussian Blue analogues on poly(diallyldimethylammonium chloride) functionalized reduced Graphene oxide

Hyojae Oh
Chemistry Education Major
Department of Science Education
The Graduate School
Seoul National University

This study reports the comparative descriptions of how hydrogen peroxide behaves with the modified electrode of poly(diallyldimethylammonium chloride)-reduced graphene oxide-prussian blue (rGO-PDDA-PB). The synthetic process of rGO-PDDA-PB was done via drop casting and electrodeposition. The electrode was modified by the dispersion of a rGO-PDDA aqueous solution, which was prepared by a thermometric synthetic process. Prussian blue was fabricated by electrochemical deposition technique on the pre-synthesized modified electrode of rGO-PDDA. The PDDA layer supports the synthetic addition of prussian blue on the surface of reduced graphene

oxide. Its electrochemical detection of hydrogen peroxide (H_2O_2) was studied by cyclic voltammetry technique. The morphology and structure of the nanocomposites on the surface of the electrode was characterized by field-emission scanning electron microscopy (FE-SEM). Its electrochemical behaviors were exhibited by amperometric responses, which was the electrocatalytic reduction behavior of hydrogen peroxide in the acidic condition of hydrochloric acid. The cyclic voltammograms of those materials has exhibited the detection of H_2O_2 according to different concentrations and scan rates. The amperometric responses have been that rGO-PDDA-FePB has shown 0.0005-0.0177mM of linear range, 738.5μA mM^{-1} cm^{-2} of sensitivity and 0.1 μM of detection limit, when rGO-PDDA-CuPB has given 0.001-0.155mM of linear range, 124.7 μA mM^{-1} cm^{-2} of sensitivity and 0.57 μM of detection limit and rGO-PDDA-NiPB has 0.0005-0.035mM of linear range, 340.3μA mM^{-1} cm^{-2} of sensitivity and 0.08 μM of detection limit. Those characteristics of rGO-PDDA-PB with different metals substituted was compared and showed the possibility of its use in applications for H_2O_2 detection.

Key words: Iron hexacyanoferrate (FePB), Nickel hexacyanoferrate (NiPB), Copper hexacyanoferrate (CuPB), Hydrogen peroxide (H_2O_2), Reduced graphene oxide (rGO), Poly(diallyldimethylammonium chloride) (PDDA)

Student Number **: 2014-22855**

Comparative study of electrochemical behavior of hydrogen peroxide using Prussian Blue analogues on poly(diallyldimethylammonium chloride) functionalized reduced Graphene oxide

1. Introduction

Carbon is one of the major components in formation of organic matter. Its ability to bind to other carbons make a various series of carbon structures such as allotropes [1-5]. According to the way the carbons assemble itself in the structure, those carbons can display different chemical and physical properties, which are shown in nanoscales, or in particular shape or even in a specific dimensions [5]. As one of the carbon structures, graphene especially, performs an outstanding properties such as mechanical, electrical, thermal and electronic characteristics and many listed in published reports [5].

In search for a material for conductive electrodes for almost 40 years, graphene has drawn significant attention from academia for a long time because of its following advantages [6]. It has high intrinsic mobility (200000cm2 v-1 s-1), a large specific surface area (2630m2g-1), high Young's modulus (~1.0TPa) and thermal conductivity (~5000Wm-1 K-1) and optical transmittance (97.7%) and good electrical conductivity [2-4, 7-13]. The sp^2 hybridization of carbon results in the structure of the graphene as the two-dimensional (2D), crystalline hexagonal lattice, which was first reported in 2004 [14]. Then it gives a strong sigma bonds, giving significant mechanical strength as well as high thermal stability due to its out-of-plane pi bonds. Graphene is also single atomic layer, honeycomb-shaped [15, 16]. the graphene has been widely used in various areas especially to sense materials electrochemically [17]. Using these properties, graphene oxide (GO) can be easily produced with various published methods such as

chemical phase exfoliation. Graphene oxide is the highly oxidized form of graphene. This graphene oxide can have its oxygens reduced to bring more restoration and the reduced graphene oxide (rGO) can make ease of functionalization of a graphene sheet. [18] However the highly hydrophobic characteristic of graphene may lead to decomposition and reassemble to graphite as its unstability. The strong van der Waals force may hinder the π-π stacking, resulting in the failure of successful usage of graphene to various electrochemical applications. [19] Considering this drawbacks of graphene, it is very important to supplement this issue because graphene has its unique properties of large specific surface area, excellent thermal stability and high electrical conductivity to enhance chemicals on its surface of the large sheets. One of main applications of the graphene oxide is on its ability to transfer electron at a fast rate and the vast redox-active surface area, which can be useful as electrochemical sensors for dopamine, ascorbic acid, caffeine, hydroquinone, and so on. Making use of electro-changes of reduced graphene oxide, charged chemical such as poly(diallyldimethylammonium chloride) (PDDA). PDDA, also shown in figure 1, is very attractive to expect strong π-π stacking effects [20]. Once positively charged PDDA is attached to graphene oxide sheet by noncovalent binding, PDDA further can bind to prussian blue by electrostatic interaction, producing $Fe(CN)_6^{3-}$ anions on rGO-PDDA.

Electrodeposition method was used for the formation of prussian blue layer on rGO-PDDA. The agglogation of prussian blue nanoparticles was assisted by the negative potentials applied in an acidic solution of ferricyanide [21-23]. Electrodeposition in an aqueous solution is an effective way to selectively deposit prussian blue at reduced graphene oxide with PDDA previously attached.

Prussian blue (FePB) of $Fe_4^{III}[Fe^{II}(CN)_6]_3$ has a structure that iron(III) attached to nitrogen and iron(II) attached to carbon [24]. Just by simply mixing the two different oxidation states, iron(II) and iron(III), in the form of ferric and hexacyanoferrate ions, a blue crystalline nanoparticles are formed to create a unit cell of a cubic structure [24, 25]. As prussian blue was found to be an excellent electrocatalyst and biosensor of reducing hydrogen peroxide and oxygen reduction [26]. This is because PB has a high selectivity for hydrogen peroxide. It is often called as "Artificial enzyme peroxidase" [32, 33]. In order to synthesize PB, there have been various ways used to synthesize and make deposition of prussian blue nanoparticles [34-36]. Many efforts have been made for even distribution and good control over the size and morphology of prussian blue. When especially the modified electrode is unstable, a simple preparation method such as electrochemical deposition of PB is very useful as it provides the controllable and rapid experimental preparation [37]. However due to its electrochemical unstability of PB on the electrode, search of many chemical supports to improve this problem was studied [38]. The method of electrodeposition of Prussian blue has been done by mixing $K_3[Fe(CN)_6]$ and $FeCl_3$. The supporting electrolyte was 0.1M KCl and 0.1M HCl. The deposition of the prussian blue film was deposited by the applied potential in the same supporting electrolyte solution by cycling the applied potential [39]. Therefore, rGO-PDDA-PB composites may improve the problems which could be caused by PB electrode, rGO electrode, or PDDA electrode.

PB has drawn much interests in academia because of its conducting zeolite structure. In recent studies, metal hexacyanoferrates also have attracted the researchers for applications in separation science [40-43],

charge storage [44-45] and corrosion protection [46].

The analogues of Prussian blues have been studied over decades. Instead of placing Fe^{3+} in the structure, it was understood that other metals were able to occupy this place such as copper, nickel, or cobalt. As the prussian blues can make ion channels connecting the transition metal and iron (III), it could be often used for easily exchangeable electrons between those metals. In those stable cycling, it was used as the redox medicator for H_2O_2 sensing. Among the prussian blue analogues with other metals exchanged, nickel (II) hexacyanoferrates (NiPB) and copper hexacyanoferrates (CuPB) have been of interest in this study as hexacyanoferrates are known as very useful electrocatalysts. With the support of nickel in the structure, nickel hexacyanoferrates provides excellent reversible and reproducible responses while nickel acts as an active cation in the zeolite structure. NiPB has been used in many applications already on conducting polymers [40], electrocatalysis [48-50], enzymatic amperometric sensors [49, 51-53, 55]. The process of deposition of NiPB is a simple method that the NiPB-modified electrodes can be easily produced. In the bulky condition of supporting electrolyte, the electrodeposition can be controlled with the applied potential and cycling numbers [56].

Similar application has been applied to CuPB. The formation of CuPB also gives the reversible and reproducible responses in the supporting electrolyte. It is viewed as the active cation for the specific application [57] and used in various applications for microsensors [58], biosensors [59] or detect hydrazine [60], amperometric sensor [61]. Prussian blue (Iron hexacyanoferrate) was found in the form of $KFe^{III}[Fe^{II}(CN)_6]$. CuPB as the form of $KCu^{II}[Fe^{II}(CN)_6]$ or

$KCu^{II}[Fe^{III}(CN)_6]$ and NiPB as the form of $KNi^{II}[Fe^{II}(CN)_6]$ or $KNi^{II}[Fe^{III}(CN)_6]$ were studied in this report. As well as the FePB and NiPB, CuPB can be electrochemically deposited on the glassy carbon electrode, which can enhance its effect to form a redox reactions and reduce hydrogen peroxide [62]. It is, however, brings unstable leakage of CuPB from the electrode surface, suggesting the need to study for an improvement. With rGO-PDDA on the electrode, the substance is still at an unstable status. At this point, the electrodeposition of prussian blue can be the successful way to complete the prussian blue deposited on rGO-PDDA. The strong specific adsorption of CN^- provide the maximum formation of prussian blue [27].

Hydrogen peroxide is one of the most common substance used for oxidizing agent. It is often considered as a by-product of oxidative metabolism [63, 64]. Also it is one of the harmful substances produced by the industrial chemistry or even from the nuclear plants that it needs to be accurately detected. [63, 64]. Therefore, various trials and studies for the detection of H_2O_2 have been done such as fluorescence [65], chemiluminescnece [66] and so on.

In this work, PDDA is a positively charged ionic polymer. The reductive need of graphene oxide was found in order to make negative atmosphere on its surface. The positive capacity of the PDDA layers [30, 68]. The negatively charged reduced graphene oxide can be stabilized with the positively charged PDDA, which can then enhance its ability to bind to prussian blue. [28-30] Therefore, the use of this nanocomposite of rGO-PDDA-PB has been used to sense hydrogen peroxide in an acidic environment and the comparison of FePB, CuPB, and NiPB in this situation were studied.

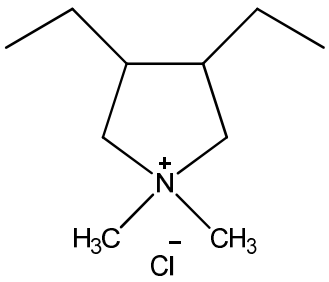

Figure 1. Chemical structure of PDDA

2. Experimental

2.1. Chemicals and reagents

Graphene oxide (highly concentrated graphene oxide dispersion in water, HC-Graphene Oxide) were used without further purification, purchased from graphene supermarket. Poly(diallyldimethylamoonium chloride) (20wt.% in H_2O), hydrogen peroxide (H_2O_2, 30 wt% in H_2O), potassium ferricyanide(III) ($K_3Fe(CN)_6$, 99+%), Iron(III) chloride ($FeCl_3$, 97%) were purchased from Sigma-Aldrich (USA). The chemicals used in this study were of analytical grade and used without further purification. All solutions used were prepared with deionized water taken from an ultrapure water purification system (Human Co., Korea) with a resistivity of not less than 18.2 MΩ cm. All measurements were carried out at room temperature.

2.2. Apparatus and measurements

Field emission scanning electron microscopy (FESEM) were performed using a SUPRA 55VP field emission scanning elecron microscope. Fourier Transform Infrared (FT-IR) spectrum was taken using Nicolet 6700 FT-IR spectrometer (from Thermo Scientific) with KBr pellet samples. Absorptions are described as the following : very

strong (vs), strong (s), medium (m), weak (w), shoulder (sh), and broad (br).

A computer-controlled CHI 842 B potentiostat was used to collect cyclic voltammetry (CV) and amperometry in a three-electrode system; For the preparation of the modified electrodes, glassy carbon working electrode (3mm diameter, GCE) was used. The working electrode for the three-electrode system was the previously prepared modified electrode. As the other electrodes of the system, a platinum (Pt) counter electrode and a silver/silver chloride (Ag/AgCl, 3 M KCl) reference electrode were used for operation. Field emission scanning electron microscopy (FESEM) measurements were performed using a SUPRA 55VP field emission scanning electron microscope, where the sample was prepared with a glassy carbon plate. Fourier transform infrared spectra (FT-IR) were recorded with a Perkin-Elmer Spectrum 2000 FT-IR spectrometer in the range of 400 – 4000 cm^{-1} using a KBr pellet. X-ray diffraction (XRD) analyses were performed on a New D8 Advance diffractometer. All ultrasonic cleaning was done using a US-2510 Ultrasonic Cleaner (Branson, USA).

2.3. Formation of rGO-PDDA nanocomposites

Functionalization and reduction of GO with PDDA was proceeded according to the following method. To prepare rGO-PDDA, 15mg of GO was dissolved in deionized water which is well dispersed previously for at least 2 hours. PDDA (0.4mL, 20wt%) was then added to the dispersed GO solution, which was then rapidly stirred and

sonicated for 1 hour until homogeneous. 0.24g of $NaBH_4$ was made into solution in 10mL DI water, which was added to the GO solution very slowly while continuous stirring. Continuous stirring was applied. Subsequently, the mixture was heated at 80 °C for 2 hours. When the reaction completed, rGO-PDDA was collected by centrifugation at 3000rpm for 1 hour until it is well washed with H2O to remove the excessive PDDA. The collected rGO-PDDA was well dried overnight in oven at 40 °C and redispersed into DI water for further use and characterization. (0.5mg/ml).

2.4. Electrochemical Preparation of rGO-PDDA-FePB nanocomposites

The rGO-PDDA nanocomposite dispersion deposited on the previously polished glassy carbon electrode and dried. Before the deposition, a glassy carbon electrode (GCE) was cleaned with 0.3 and 0.5 μm alumina slurry and rinsed thoroughly with deionized water. It was then ultrasonicated in deionized water for 3 mins twice. When the clean electrode was well dried in air, 5μL of rGO-PDDA nanocomposite dispersion (0.5mg/ml) was dropped on the surface of the electrode and dried at 40 °C for at least 2 hours.

In a electrolytic cell, $FeCl_2$ (4mM, 5mL) and $K_3[Fe(CN)_6]$ (4mM, 5mL) was prepared in 0.1mol/L KCl + 0.01mol/L HCl with the electrode of rGO-PDDA deposited. A cathodic current was applied to it with the potential of 0.5 to －0.2V between cyclic voltammetry scan 25

laps (sweep rate of 50mV/s). As shown in figure 10, the cyclic voltammogram (CV) showed the successful electrodeposition of rGO-PDDA-FePB. This range of the applied potential was decided after several trials.

2.5. Electrochemical Preparation of rGO-PDDA-CuPB and rGO-PDDA-NiPB nanocomposites

The electrodeposition of rGO-PDDA-CuPB and rGO-PDDA-NiPB was prepared by the preparation of a rGO-PDDA electrode as mentioned in section 2.3. But in the electrolytic cell, rGO-PDDA-CuPB had $CuCl_2$ (4mM, 5mL) and $K_3[Fe(CN)_6]$ (4mM, 5mL) in 0.1mol/L KCl + 0.01mol/L HCl with the potential from 0.95V to －0.4V between cyclic voltammetry scan 25 laps (sweep rate of 50mV/s. For rGO-PDDA-NiPB had $NiSO_4 \cdot 6H_2O$ (4mM, 5mL) and $K_3[Fe(CN)_6]$ (4mM, 5mL) in 0.1mol/L KCl + 0.01mol/L HCl in the electrolytic cell. The applied potential was 0.75 to 0.05V between cyclic voltammetry scan 50 laps (sweep rate of 50mV/s). This is shown in figure 11 and 12.

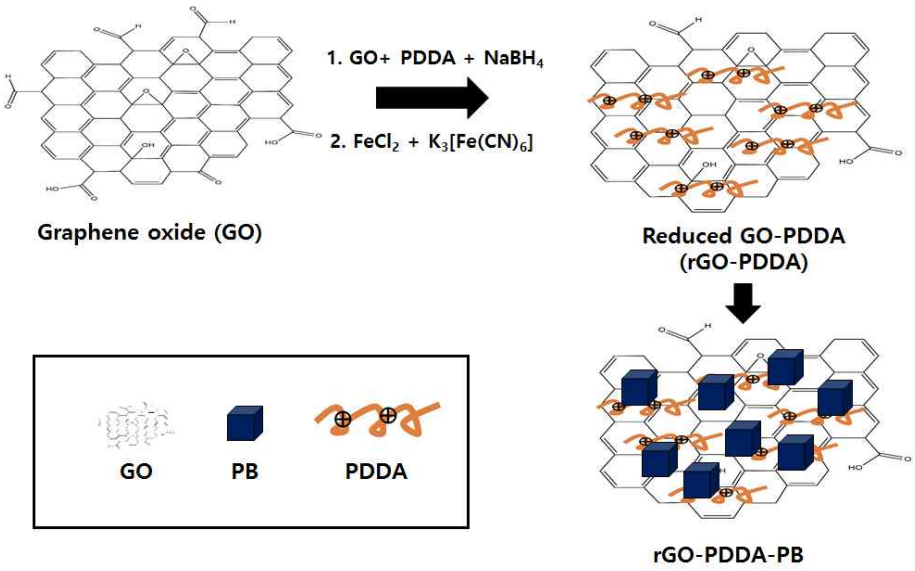

Figure 2. Demonstrated scheme of the synthesis of rGO-PDDA-PB.

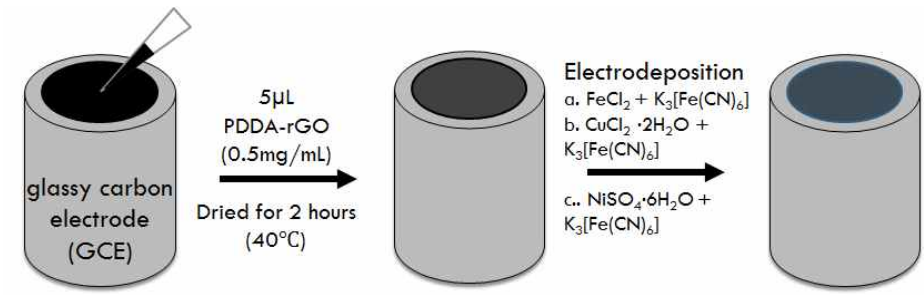

Figure 3. Scheme of the experimental procedure of rGO-PDDA and electrodeposition.

3. Results and Discussion

3.1. Characterization and comparison of the rGO-PB and rGO-PDDA-PB nanocomposites

The synthesis process of rGO-PDDA-PB has been exhibited in figure 2. The nanoparticles were prepared by the synthetic processes. The as-synthesized graphene oxide was first prepared in the neutral condition with distilled water. The strong alkaline agent, sodium borohydride was used to make alkaline condition of the solution of graphene oxide. In order to prepare rGO-PDDA composites, prepared GO solution and PDDA solution were mixed with addition of reducing agent, sodium borohydride. The reduced graphene oxide and assisted PDDA were then synthesized on the surface of graphene oxide [69-71].

Next, the morphology of the nanocomposites were observed using the SEM images. In order to compare the existence of prussian blue nanoparticles on the surface, the SEM images were taken. The figure has shown the successful. It was archived that the π-π stacking between the delocalized sp^2 carbon structure of graphene and the crystalline structured molecules bound to prussian blue nanoparticles. The graphene oxide is composed of the delocalized sp^2 carbon structure. The π-π stacking interaction was obtained between the delocalized sp2 carbon structure and the prussian blue nanostructures. This indicates that PDDA played an important role in binding prussian blue nanoparticles on the reduced graphene oxide sheets. This graphene

sheet with PDDA and prussian blue were observed with SEM images, by simulating exactly the same experimental environment. A glassy carbon plate was coated with 5μl of rGO-PDDA solution (0.5mg/ml). After air-drying it on the film, the glassy carbon plate was modified by electrochemically deposition after several cycles according to each conditions for FePB, NiPB, and CuPB electrodeposition.

Although the morphology of the rGO-PDDA-PB was not clearly seen on the SEM images, it is archieved that the PB nanoparticles were well capped on the surface of the graphene oxide. There are not much clear difference on the SEM images between rGO-PDDA and rGO without any modification of PDDA on its surfaces. However when the PB were synthesized on either rGO-PDDA or rGO, some of PB nanoparticles were observed. We observed much more PB nanoparticles captivated on rGO-PDDA than on rGO sheets. This indicates PDDA plays an important role in assisting Prussian Blue to effectively self-assembly on the functionalized graphene oxide sheet.

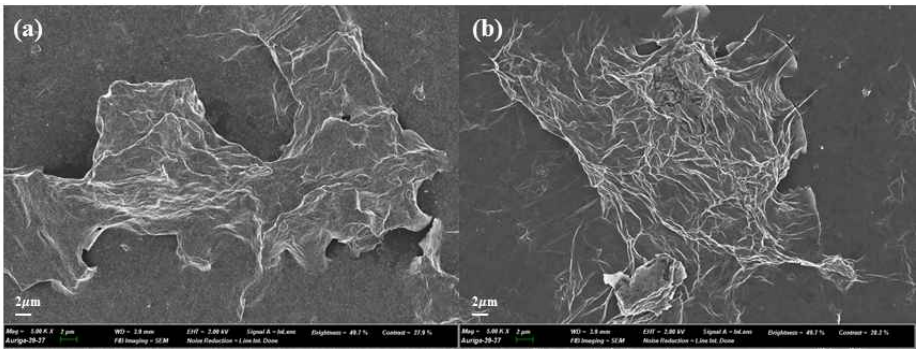

Figure 4. SEM images of (a) rGO-PDDA and (b) rGO at different magnifications.

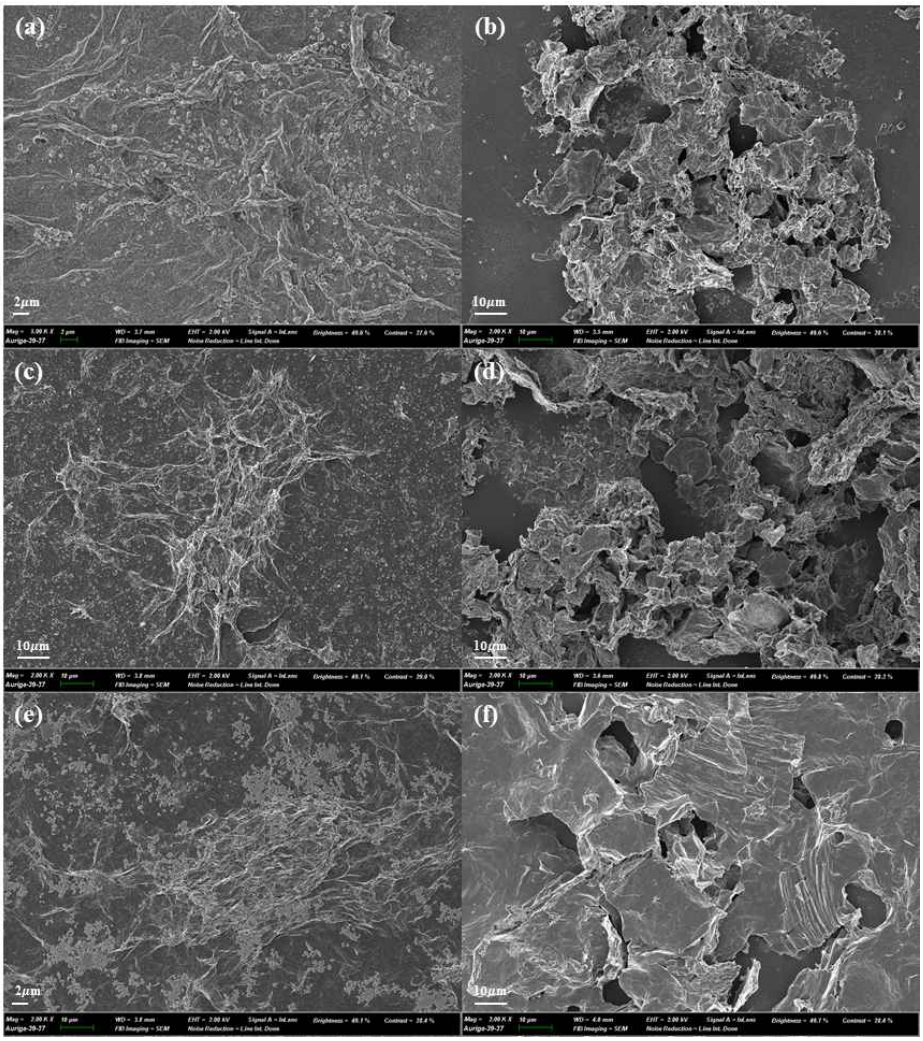

Figure 5. SEM images of (a)rGO-PDDA-FePB, (b) rGO-FePB, (c) rGO-PDDA-CuPB, (d) rGO-CuPB, (e) rGO-PDDA-NiPB, (f) rGO-NiPB nanocomposites at different magnifications with comparisons of PB existence.

The morphology and size of nanocomposites were characterized by the SEM images. The synthesis of PB nanoparticles was processed on the surface of the glassy carbon plate, modified with rGO or rGO-PDDA. The analysis of the SEM images confirms that Prussian Blue nanoparticles were densely packed onto the PDDA-modified graphene oxide sheets. Although the size of prussian blue depends on various factorsuch as its rate of nucleation or small changes of ionic concentrations and so on, The sizes of the FePB nanoparticles on the SEM images are close to consistency [72]. The size of the FePB particles was about 0.7μm, taken from the SEM images (fig. 5).

As shown in the scheme of the formation mechanism of rGO-PDDA-PB and rGO has been stored in an acidic condition (0.01M of hydrochloric acid in 0.1M potassium chloride) (Fig. 2). As the scheme of the synthetic mechanism of rGO-PDDA-PB nanocomposites is shown in the following figure (Fig. 2), it was prepared with the one-pot synthesis method according to the following literatures. In order to reduce GO, the reducing agent, sodium borohydride was used. The purchased well mixed GO solution was sonicated to make sure its homogeneity for about 1 hour. The PDDA monomer was added to the dispersed solution of GO. About extra 15 minutes of another sonication, the reducing agent, sodium borohydride was slowly added. Slight separation of solution was observed. The solution was immersed in a 80 ℃ oil bath and heated for at least 2 hours with steady stirring to ensure that the polymerization took placed adequately. Throughout this process, the PDDA polymer were onto the reduced graphene oxide and had π-π interaction polymerized on reduced graphene oxide [31, 47].

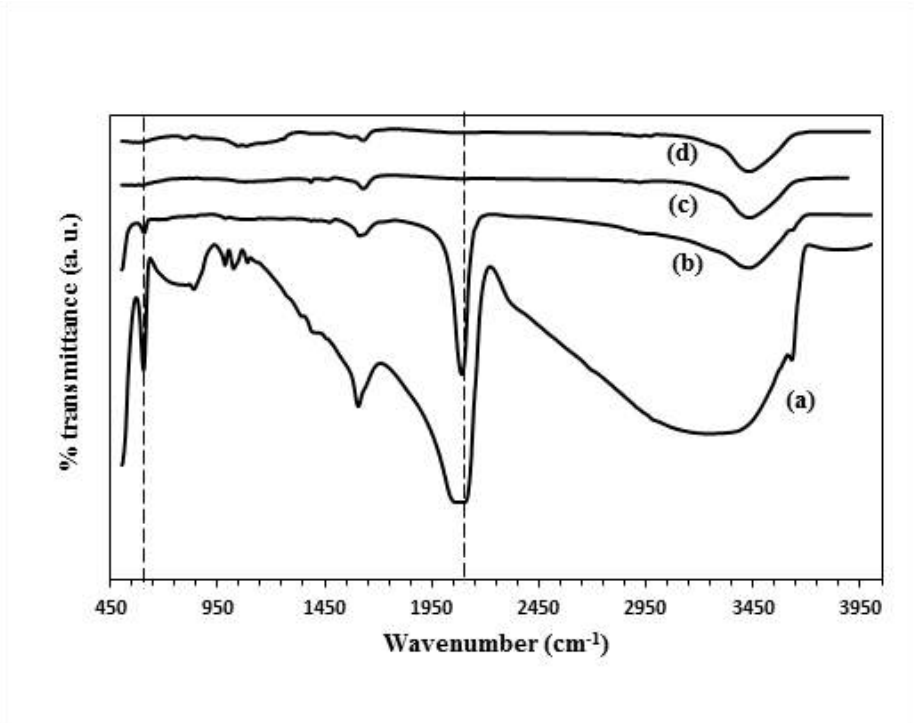

Figure 6. FT-IR spectra of (a) FePB, (b) rGO-PDDA-FePB nanocomposites, (c) rGO-PDDA, (d) rGO

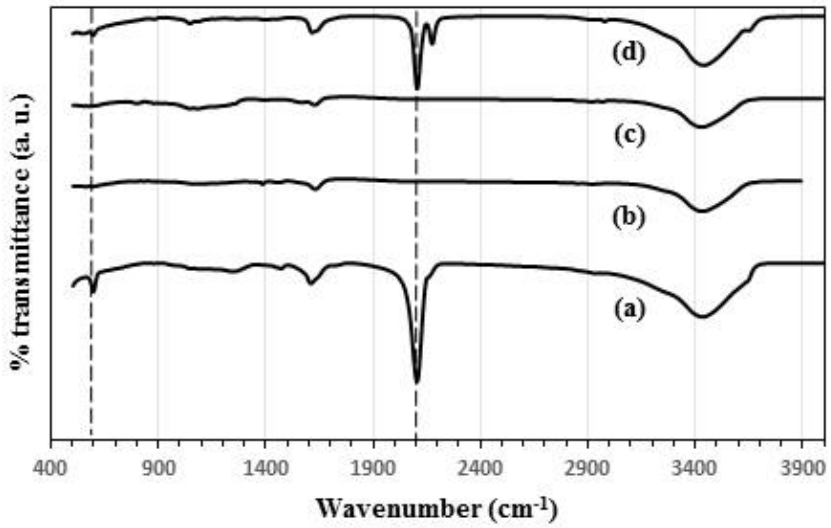

Figure 7. FT-IR spectra of (a) rGO-PDDA-CuPB nanocomposites, (b) rGO-PDDA, (c) rGO, (d) CuPB

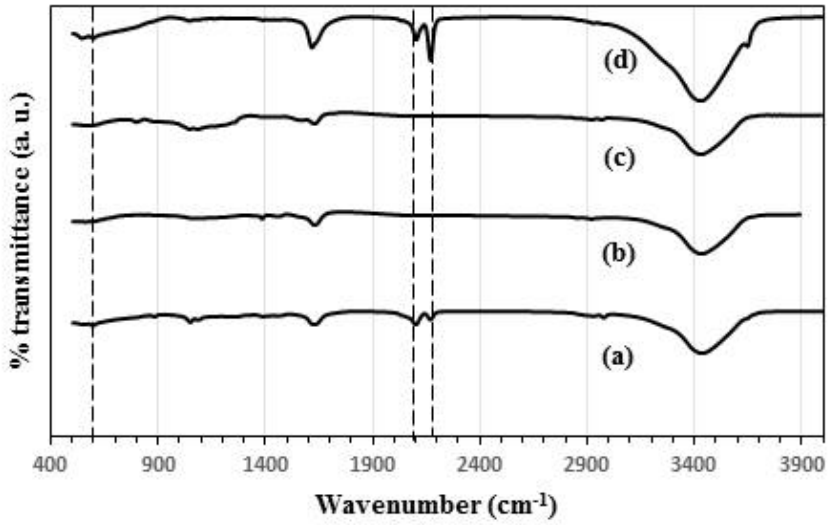

Figure 8. FT-IR spectra of (a) rGO-PDDA-NiPB nanocomposites, (b) rGO-PDDA, (c) rGO, (d) NiPB

The chemical functional groups have been investigated further using FT-IR, shown in fig 6, 7 and 8. Fig. 6 shows the FT-IR spectrum of FePB, rGO-PDDA, rGO and rGO-PDDA-FePB. Although the noise have been observed in FePB peaks only, it is clear to see C≡N stretching of [Fe^{II}-CN-Fe^{III}] structure at 2073 cm^{-1} (fig. 6). The formation of [Fe^{II}-CN-Fe^{III}] is also observed in 601.36 cm^{-1}. For absorption peaks for rGO-PDDA, the distinctive peaks are shown at 1466.00 cm^{-1} of weak absorption for $–CH_2$ and 1081.20 cm^{-1} of weak absorption for C-N. Also for rGO, the corresponding peak is observed at C=C at 1630.11 cm^{-1}. For rGO-PDDA-FePB, the C≡N stretching of [Fe^{II}-CN-Fe^{III}] is also observed at 2085.74 cm^{-1} as well as C=C bond for rGO at 1608.24 cm^{-1} and formation of [Fe^{II}-CN-Fe^{III}] is shown at 603.39 cm^{-1}. From figure 7, C≡N stretching peaks of [Cu^{II}-CN-Fe^{III}] for copper hexacyanoferrate was at 2102.11 cm^{-1} and 2171.75 cm^{-1}. The formation peak was shown at 592.88cm^{-1}. This two peaks are due to the mixed formation of Cu(II) and Cu(III). For rGO-PDDA-CuPB, the C≡N stretching of [Cu^{II}-CN-Fe^{III}] is also observed at 2101.20 cm^{-1} when the C=C banding for rGO at 1607.02 cm^{-1} and formation of [Cu^{II}-CN-Fe^{III}] is shown at 594.55 cm^{-1}. From figure 8, the C≡N stretching of [Ni^{II}-CN-Fe^{III}] was located at 2098.19 and 2166.83 cm^{-1}. Also the formation of the [Ni^{II}-CN-Fe^{III}] was at 593.90 cm^{-1}, where the assigned C≡N stretching for rGO-PDDA-NiPB was at 2066.33 and 1625.23 cm^{-1}. The formation of [Ni^{II}-CN-Fe^{III}] was observed at 591.85cm^{-1}. This C=C stretching vibration located around 1600-1630 cm^{-1} shows that rGO is well attached with prussian blue. The peaks observed indicate the formation of rGO-PDDA-PB.

3.2. Potentiodeposition of FePB, CuPB, NiPB on rGO-PDDA modified GCE

In order to successfully deposit the PBs on the rGO-PDDA modified GCE. Many other methods were tried in advanced and found the best method. Simple mixing method was not successful that the PBs were broken only after some short time of applying potential, as shown in the rapidly decreased peak currents and dramatic changes of peak locations. As a solution to this problem, the electrodeposition was carried out with cyclic voltammetric method. Also, the purpose of comparing prussian blues of different metals in H_2O_2 detection, the experimental conditions were optimized for each PB. First, for iron hexacyanoferrates, the electrodeposition was carried out with cyclic voltammetric method in a solution of 0.1 M KCl and 10mM HCl with 0.002 M $FeCl_2$ and 0.002 M $K_3[Fe(CN)_6]$ (fig. 9). The cyclic potential sweep was between 0.5 to 0.2 V with 25 scan laps at a scan rate of $50mVs^{-1}$. With the potential sweep going on, the peak currents of cyclic voltammograms (CVs) increased at 0.17 V and 0.23 V because of the gradual formation of FePB on the modified electrode. As it processed, the increasing peaks were stabilized and the peaks were no longer increased at the end of the cycles. After cycling several more times, it was made sure that the cycling went to the maximum in its growth. This growth of iron hexacyanoferrates in interacting with PDDA-rGO was confirmed as shown in the following figure (fig.9).

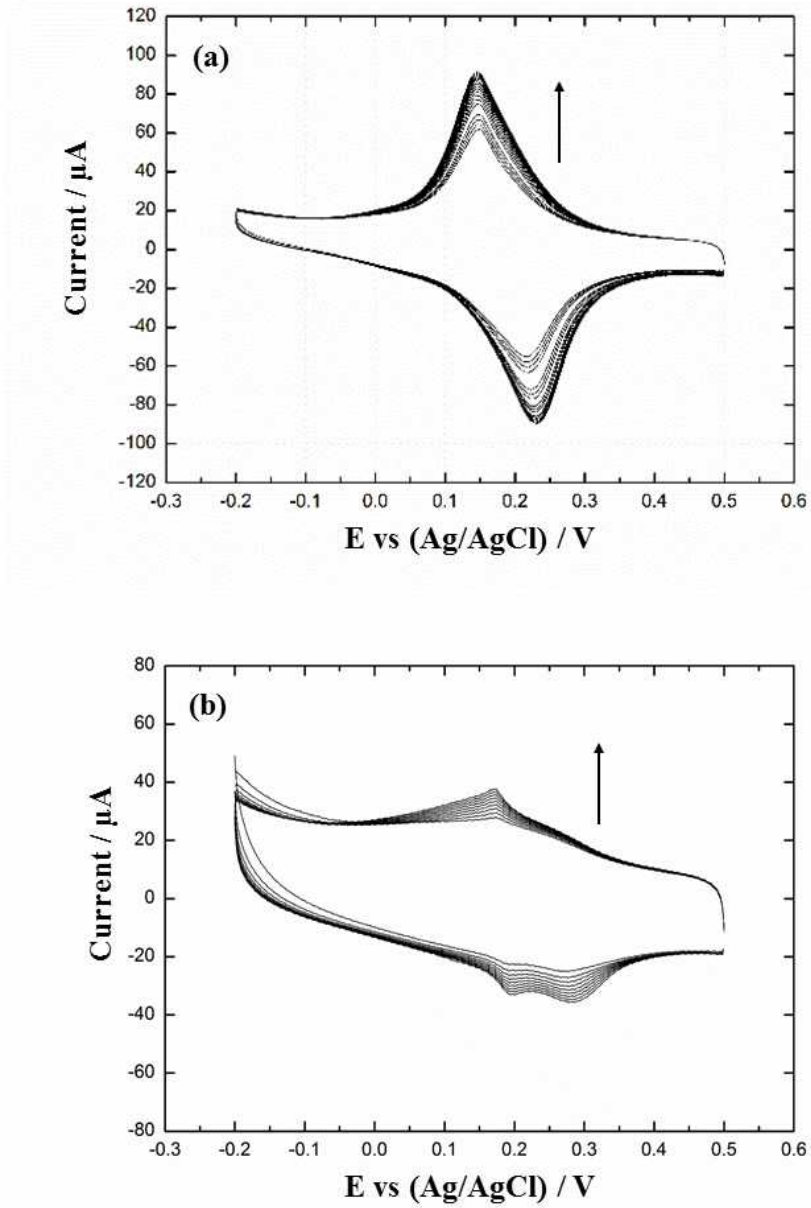

Figure 9. CVs of (a) FePB electrodeposition on rGO-PDDA electrode, (b) FePB electrodeposition on rGO electrode in a solution of 0.1M KCl and 10mM HCl

The cyclic volammetry was also applied in order to proceed the electrodeposition of other metal hexacyanoferrates. For cupper hexacyanoferrate (CuPB) on rGO-PDDA modified electrode or rGO-PDDA-CuPB, a solution of 0.002 M $CuCl_2 \cdot 2H_2O$ and $K_3[Fe(CN)_6]$ was prepared in a solution of 0.1 M KCl and 10mM HCl. The cyclic potential was applied between 0.95 V to – 0.4 V with scan of 25 laps at a sweep rate of 50 mVs^{-1}. Same procedure was applied to the rGO modified electrode instead of rGO-PDDA electrode. Without PDDA on rGO, the potential current could not be higher than 60 μA when the highest rGO-PDDA-CuPB went uptil 100μA. Overall, the peak currents raised, which is similar to FePB formation. This increase showed the formation of CuPB as shown in figure 10. For NiPB formation on PDDA-rGO formation (fig. 11), a 20ml solution of 0.002M $NiSO_4 \cdot 6H_2O$ and $K_3[Fe(CN)_6]$ was used as the electrolyte. They were also prepared in solution of 0.1 M KCl and 10mM HCl. The cyclic potential was between 0.75V to 0.05V between cyclic voltammetry scan 50 laps at a sweep rate of 50mVs^{-1}. This was also repeated for rGO-NiPB, which was observed with similar peak location or its electrochemical transform. However as more potential was applied during the rGO-NiPB formation, no more increase of peak current was observed and distruction of the peaks was observed at some times.

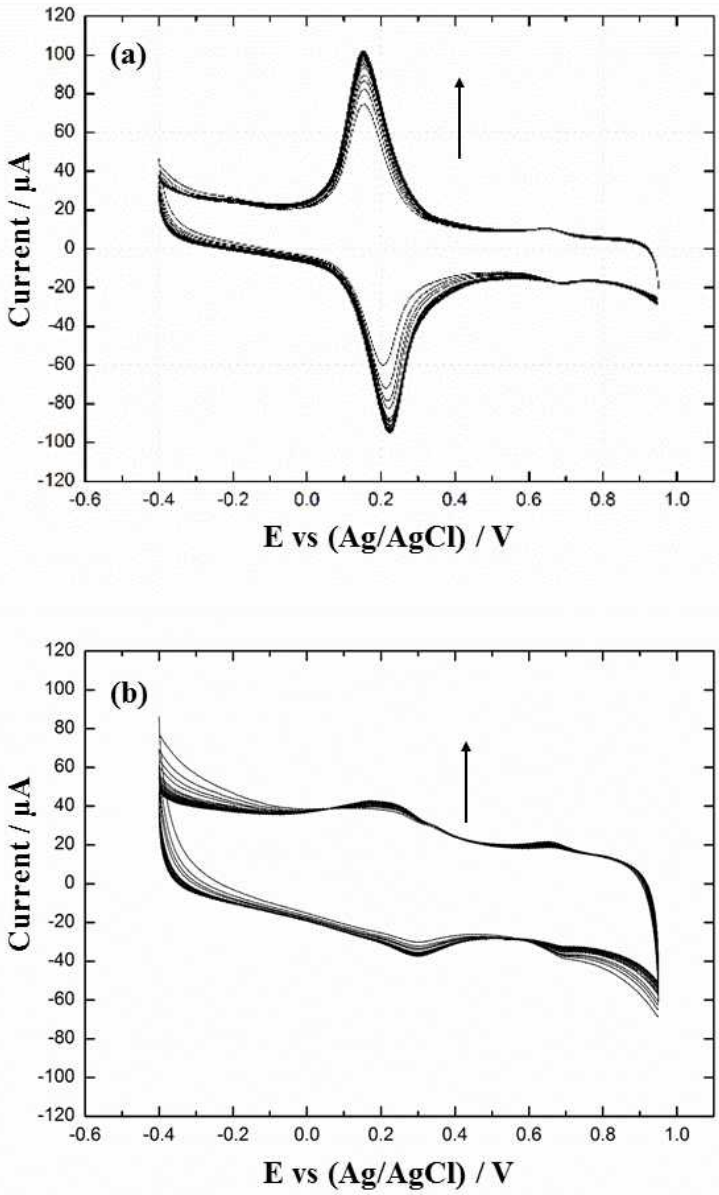

Figure 10. CVs of (a) CuPB electrodeposition on rGO-PDDA electrode, (b) CuPB electrodeposition on rGO electrode in 0.1M KCl + 10mM HCl

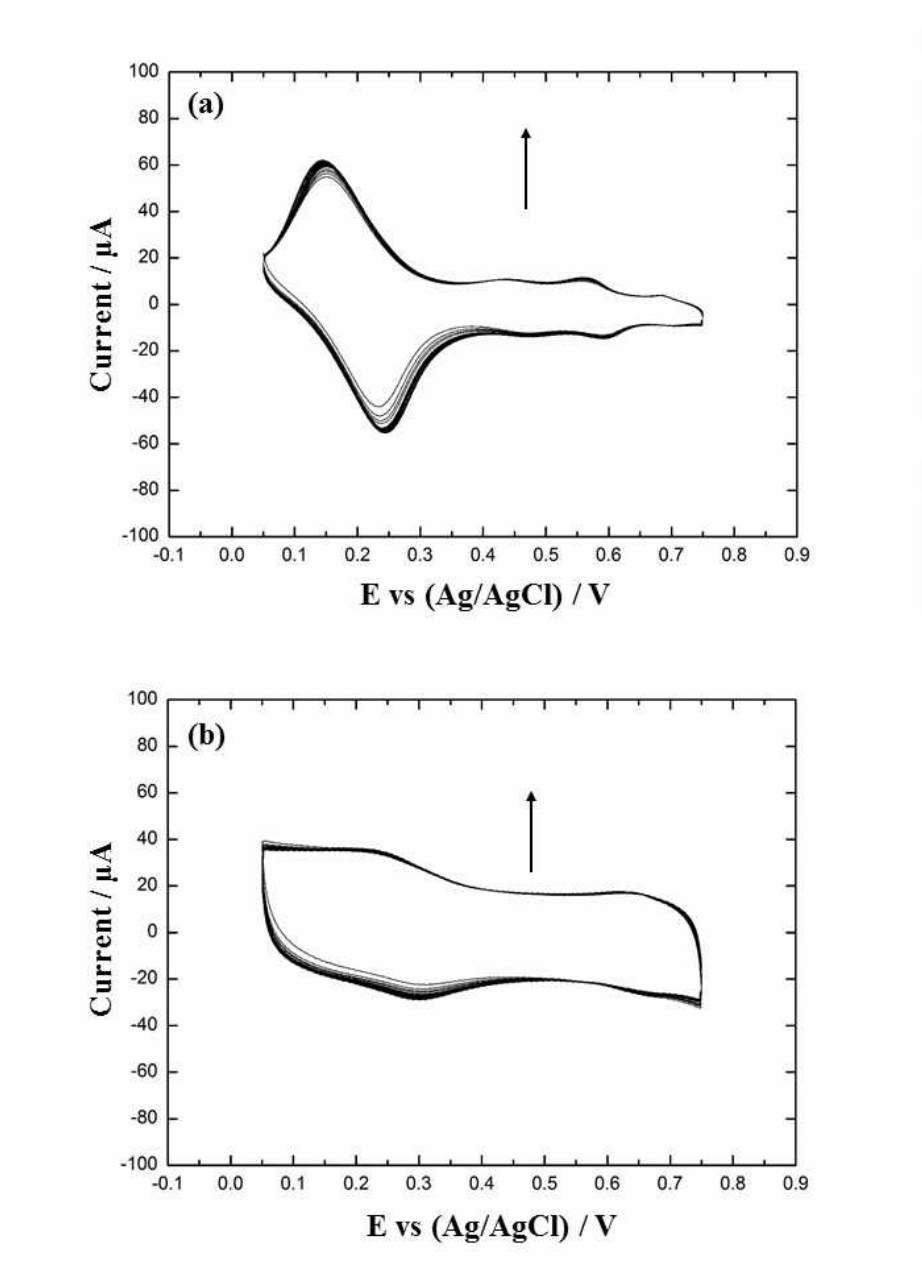

Figure 11. CVs of (a) NiPB electrodeposition on rGO-PDDA electrode, (b) NiPB electrodeposition on rGO electrode in 0.1M KCl + 10mM HCl

After the addition of $Fe(CN)_6^{3-}$ to the solution of interest, the synthesis of $Fe(CN)_6^{3-}$ anions on the surface of the composite happens. At this process, the electrostatic interaction works due to the positive charge of PDDA at rGO-PDDA and its attraction towards anion. This process may be called of smooth binding of Fe^{3+} and $Fe(CN)_6^{3-}$ on the surface of rGO-PDDA modified electrode, resulting $Fe^{III}-Fe^{III}(CN)_6^{3-}$. Considering that prussian blue is formed by the combination of Fe^{3+} and $Fe(CN)_6^{3-}$, this chemistry happens with copper hexacyanoferrate formation process where CuPB is the coordination of Cu^{2+} and $Fe(CN)_6^{3-}$. [54, 67] Due to the electron transfer in the formation of $Fe^{III}-Fe^{III}(CN)_6^{3-}$, hydrogen peroxide reduction may be possible at an easy control of applied potential. Especially the electrochemically deposition happens well at an acidic condition because ferricyanide ion and the free iron ions (Fe^{3+} and Fe^{2+}) process through exchangeable redox reactions, which indicate that ferricyanide experience dissociation process in such acidic condition [23, 77].

3.3. Volummetric response of H_2O_2 at rGO-PDDA-PB

The cyclic voltammetry peaks were studied in comparing the phenomena the bare GCE, rGO, rGO-PDDA, rGO-FePB, and rGO-PDDA-FePB modified glassy carbon electrode. Fig. 12 was drawn to illustrate the effect of FePB and PDDA on its redox reactions in the bare condition in a 0.1M KCl aqueous solution in the presence of 10mM hydrochlorid acid. The reversible pair of the redox peaks for rGO-PDDA-FePB was increased than other compared electrodes. For rGO glassy carbon electrode (Fig. 12 (b)), the redox peaks were shown higher than the peaks for rGO-PDDA (Fig. 12 (c)). However those peaks were almost negligible, compared to the redox peaks for rGO-PDDA-FePB (Fig. 12 (e)). The same phenomena was observed in the one of CuPB and NiPB. However it seems that the redox peaks for rGO-PDDA-CuPB and rGO-PDDA-NiPB were shown at higher currents, where almost no redox pair peaks were observed for the bare GCE (fig. 12 (a), fig. 13 (a), fig. 14 (a)) The reversible peaks for rGO-PDDA-PB (fig. 12 (e), fig. 13 (e), fig. 14 (e)) were observed to be well-defined. The rGO peaks were rather higher at currents than the peaks for rGO-PDDA, probably due to rather less stability of rGO-PDDA due to higher electrocharges and electrical conductivity of PDDA on the surface of rGO. From this observation, PB nanoparticles play an important role in excellent electrocatalytic activity to reduce H_2O_2. However the more detailed work on comparison may be needed in the further investigation in the later part.

In regards to the previous studies, the electrocatalytic process of prussian blue can be demonstrated as below [73]:

$$Fe^{III}[Fe^{II}(CN)_6]\ (PB) + K^+ + 4e^- \rightarrow K_2Fe^{II}[Fe^{II}(CN)_6]\ (PW) \quad (1)$$

$$2K_2Fe^{II}[Fe^{II}(CN)_6]\ (PW) + H_2O_2 + 2H^+ \rightarrow 2KFe^{III}[Fe^{II}(CN)_6]\ (PB) + 2H_2O + 2K^+ \quad (2)$$

$$2K_2Cu^{II}[Fe^{II}(CN)_6]\ (PW) + H_2O_2 + 2H^+ \rightarrow 2KCu^{III}[Fe^{II}(CN)_6]\ (PB) + 2H_2O + 2K^+ \quad (3)$$

$$2K_2Ni^{II}[Fe^{II}(CN)_6]\ (PW) + H_2O_2 + 2H^+ \rightarrow 2KNi^{III}[Fe^{II}(CN)_6]\ (PB) + 2H_2O + 2K^+ \quad (4)$$

As shown in the above equations, PB is easily reduced to Prussian white (PW), when referred to equation (1). On the surface of the electrode, the electron transfer occurs so that the PB is reduced to PW and PW is reoxidized to PB with the support of H_2O_2. With the help of H_2O_2 as a role of electrocatalyst, PB, the redox peaks increased in the amount of currents in the CVs, explained by equation (2). The equation (3) and (4) shows how CuPB and NiPB reduces hydrogen peroxide. This process can be observed in figure 15, 16 and 17 with the presence of 1mM H_2O_2 in the electrolyte solution.

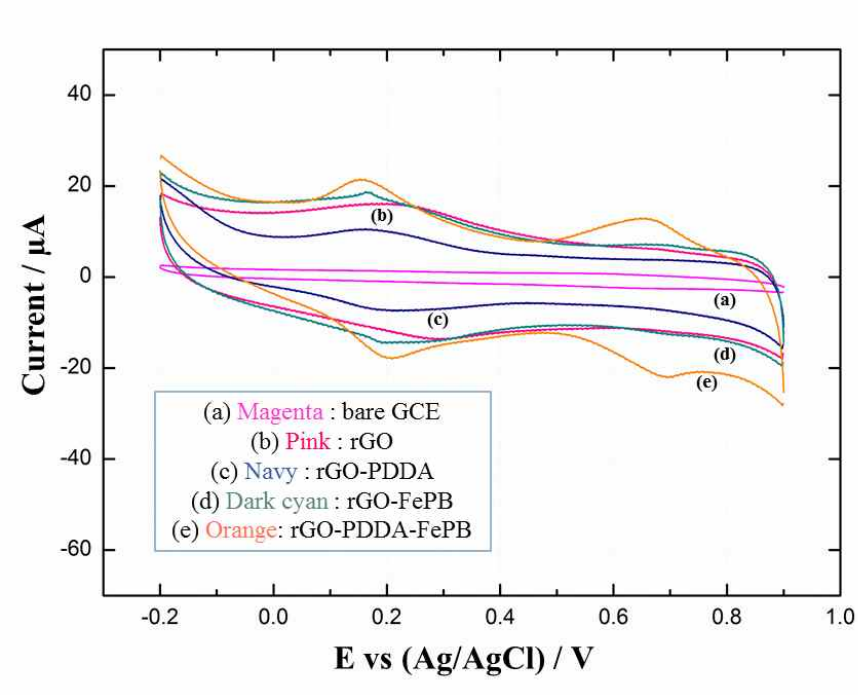

Figure 12. CVs of (a) Bare GCE, (b) rGO, (c) rGO-PDDA, (d) rGO-FePB, (e) rGO-PDDA-FePB on a glassy carbon electrode in 0.1M KCl aqeuous solution with 10mM HCl at a scan rate of 50mVs^{-1}.

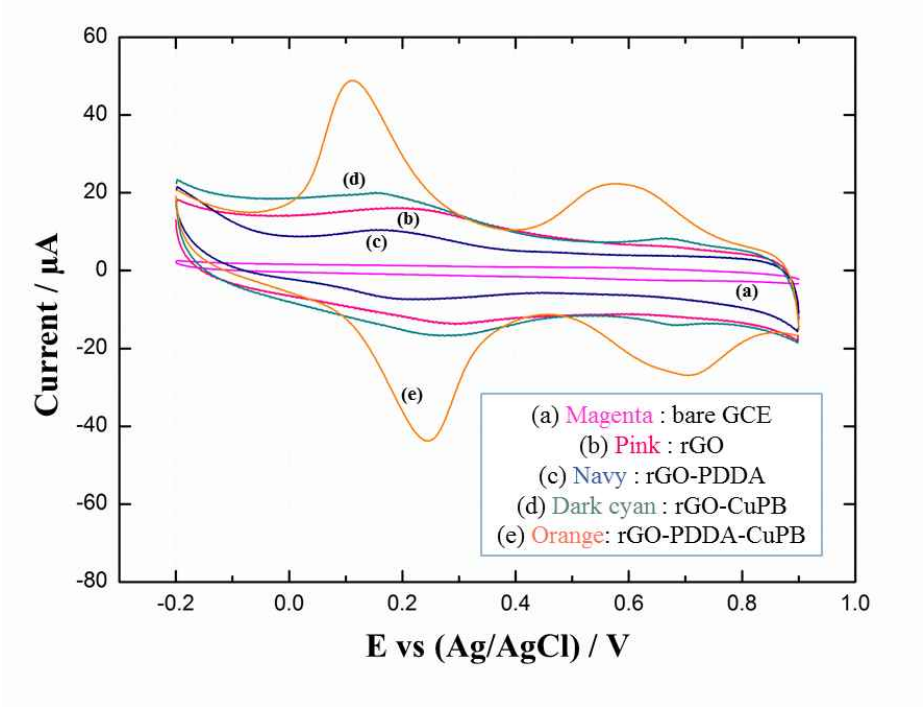

Figure 13. CVs of (a) Bare GCE, (b) rGO, (c) rGO-PDDA, (d) rGO-CuPB, (e) rGO-PDDA-CuPB on a glassy carbon electrode in 0.1M KCl aqeuous solution with 10mM HCl at a scan rate of 50mVs^{-1}.

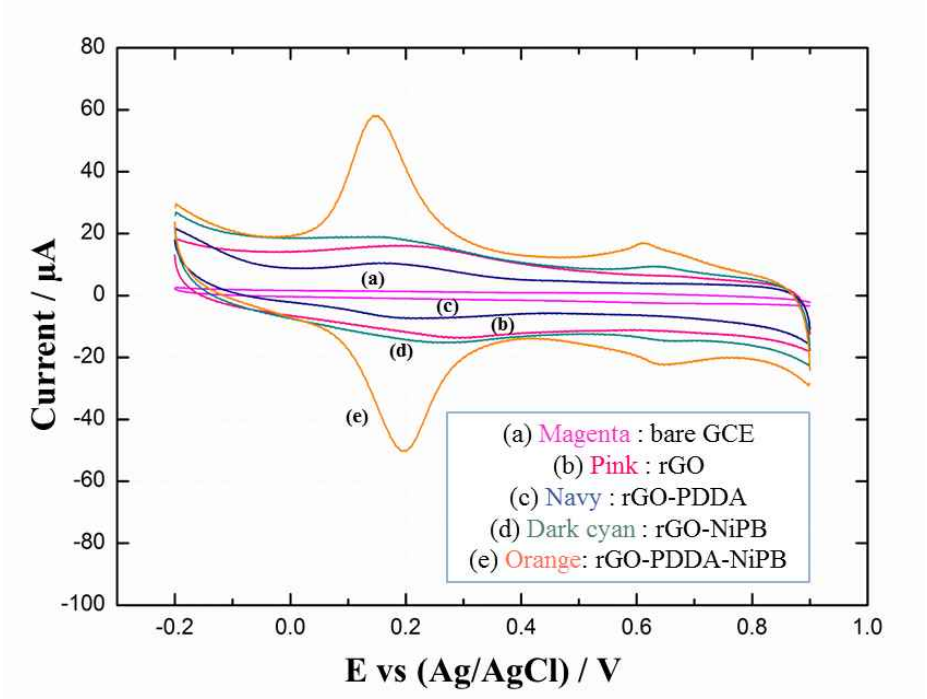

Figure 14. CVs of (a) Bare GCE, (b) rGO, (c) rGO-PDDA, (d) rGO-NiPB, (e) rGO-PDDA-NiPB on a glassy carbon electrode in 0.1M KCl aqeuous solution with 10mM HCl at a scan rate of 50mVs^{-1}.

The effect of H_2O_2 concentration to rGO-PDDA-PB and the effect of scan rates on rGO-PDDA-PB at a constant H_2O_2 concentration were investigated using CVs in figure 15 to figure 20. Figure 15 (A) displays the CV of rGO-PDDA-FePB in a 0.1M KCl aqueous solution with 10mM HCl at a scan rate of $50mVs^{-1}$. As the H_2O_2 concentration increases, the cathodic current peak was constantly increased. In comparison to that, figure 15 (B) shows that rGO-FePB has not as good cathodic current peak as the peaks for rGO-PDDA-FePB. Figure 16 shows the cyclic voltammograms of rGO-PDDA-CuPB and rGO-CuPB in 0.1M KCl aqueous solution with 10mM HCl at a scan rate of $50mVs^{-1}$ constant increasing cathodic current peak as well. he constant increase of cathodic current peak was observed for rGO-PDDA-CuPB and rGO-CuPB (fig. 16) and rGO-PDDA-NiPB and rGO-NiPB (fig. 17).

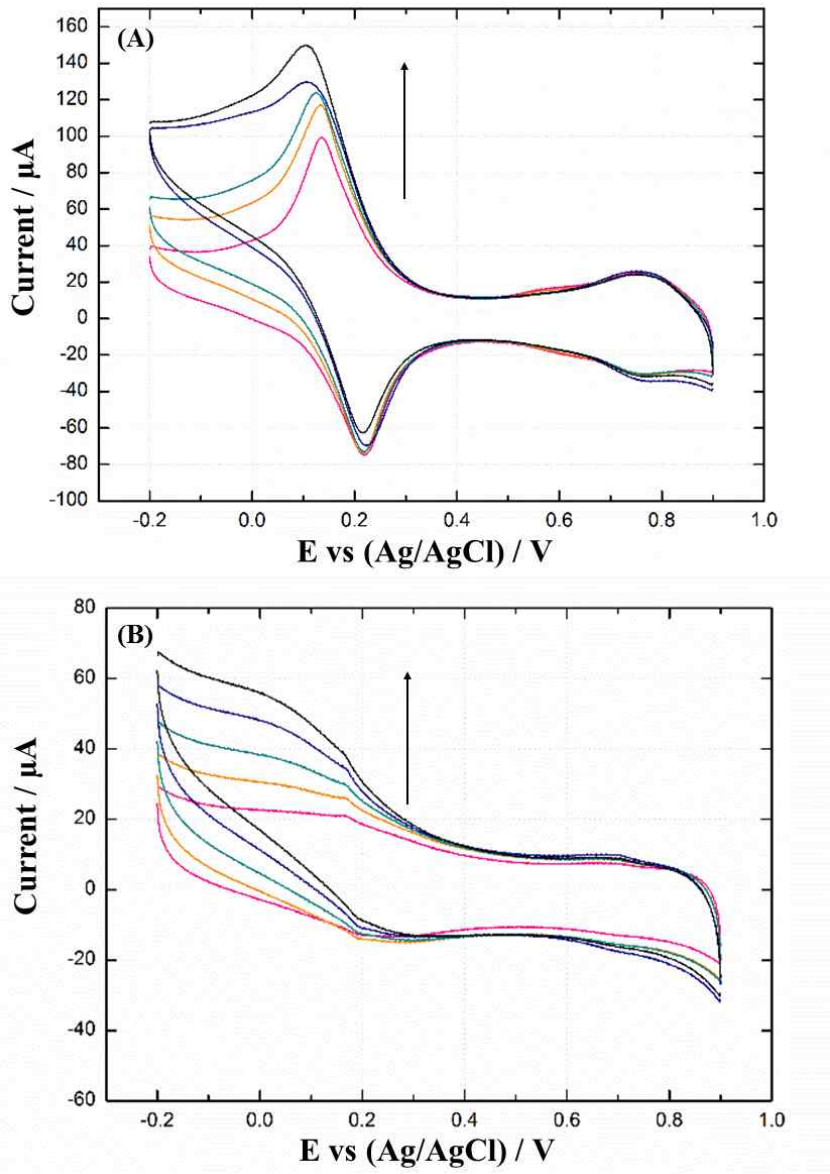

Figure 15. CVs of (A) rGO-PDDA-FePB in the increasing H_2O_2 concentration (1mM, 2mM, 3mM, 4mM, 5mM) (B) rGO-FePB in the increasing H_2O_2 concentration (1mM, 2mM, 3mM, 4mM, 5mM) in 0.1M KCl aqeuous solution with 10mM HCl at a scan rate of $50mVs^{-1}$.

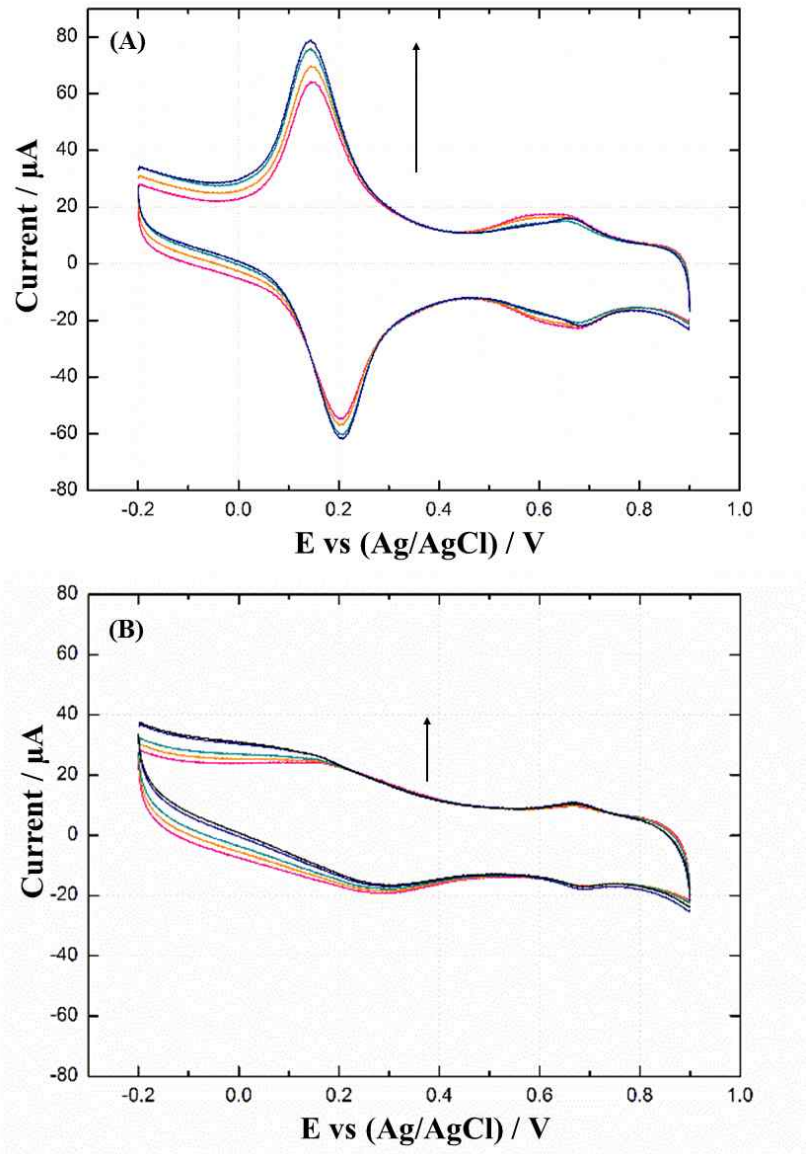

Figure 16. CVs of (A) rGO-PDDA-CuPB in the increasing H_2O_2 concentration (1mM, 2mM, 3mM, 4mM, 5mM) (B) rGO-CuPB in the increasing H_2O_2 concentration (1mM, 2mM, 3mM, 4mM, 5mM) in 0.1M KCl aqeuous solution with 10mM HCl at a scan rate of $50mVs^{-1}$.

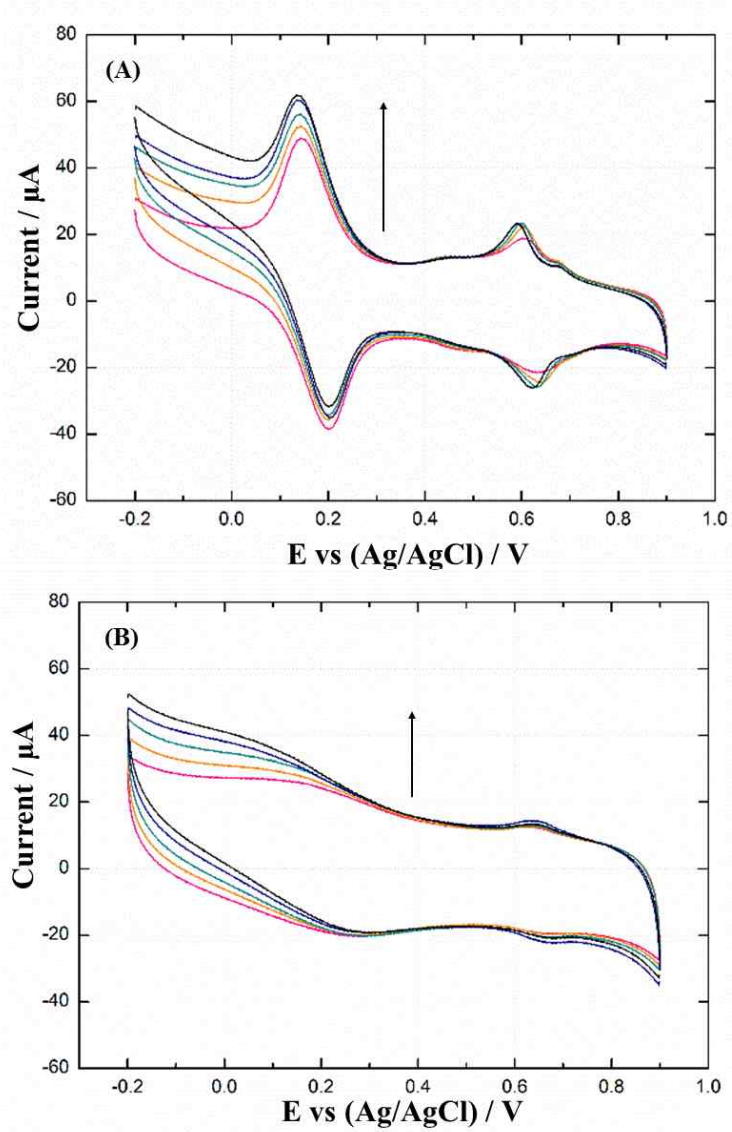

Figure 17. CVs of (A) rGO-PDDA-NiPB in the increasing H_2O_2 concentration (1mM, 2mM, 3mM, 4mM, 5mM) (B) rGO-NiPB in the increasing H_2O_2 concentration (1mM, 2mM, 3mM, 4mM, 5mM) in 0.1M KCl aqeuous solution with 10mM HCl at a scan rate of $50mVs^{-1}$.

From figure 18, the cyclic voltammogram of rGO-PDDA-FePB was done in 0.1M KCl aqueous solution with 10mM HCl solution in the presence of 1mM H_2O_2 with different scan rates increasing from 10, 20, 50, 100, 200 mVs^{-1}. The constant increase of the cathodic peak was observed as the scan rates were increased. It was displayed as the correlation coefficient of 0.9930 (inserted in fig. 18). Figure 19 also exhibits the cyclic voltammogram of rGO-PDDA-CuPB in 0.1M KCl aqueous solution with 10mM HCl with 1mM H_2O_2 at different scan rates (from 10, 20, 50, 100, 200 mVs^{-1}). This cyclic voltammogram shows a linear relationship with the constant hydrogen peroxide concentration with the correlation coefficient of 0.9882 (inset in fig. 19). Figure 20 displays the relationship between the current and the scan rate for rGO-PDDA-NiPB. The scan rates were increased at the scan rates of 10, 20, 50, 100, and 200 mVs^{-1}. The graph of the correlation was inserted inside the figure 10, which indicated that correlation coefficient was 0.9867.

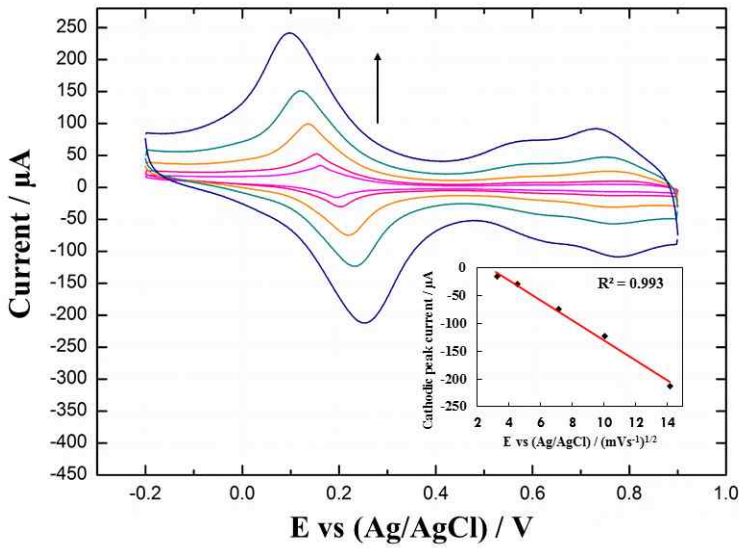

Figure 18. CVs of rGO-PDDA-FePB in 0.1M KCl aqueous solution with 10mM HCl solution in the presence of 1mM H_2O_2 with different scan rates (from 10, 20, 50, 100, 200 mVs^{-1})

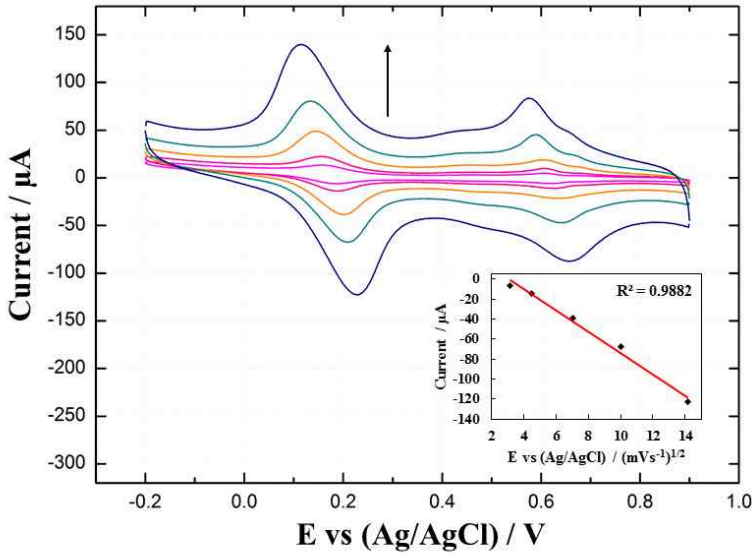

Figure 19. CVs of rGO-PDDA-CuPB in 0.1M KCl aqueous solution with 10mM HCl solution in the presence of 1mM H_2O_2 with different scan rates (from 10, 20, 50, 100, 200 mVs^{-1})

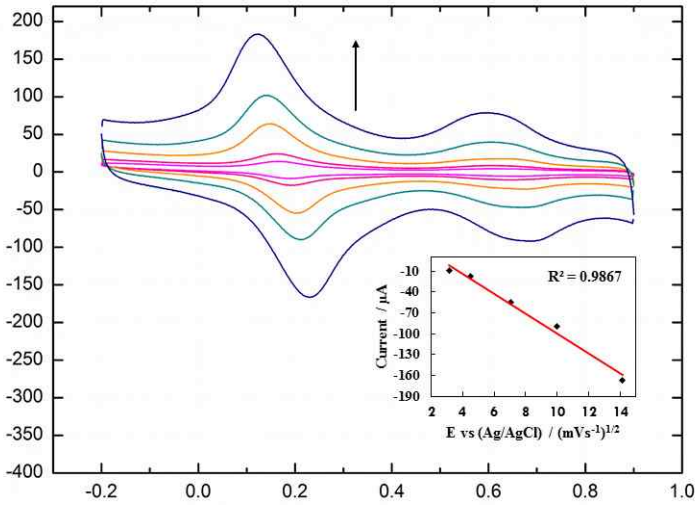

Figure 20. CVs of rGO-PDDA-NiPB in 0.1M KCl aqueous solution with 10mM HCl solution in the presence of 1mM H_2O_2 with different scan rates (from 10, 20, 50, 100, 200 mVs^{-1})

3.4. Amperometric response of H_2O_2 at rGO-PDDA-PB

The amperometric responses of rGO-PDDA-FePB was displayed in figure 21. As shown in this figure, the injection of H_2O_2 was done in 0.1M KCl + 10mM HCl with the applied potential of +0.17V. The peaks are the responses for each injection of H_2O_2. After the injection of H_2O_2, it reached a steady current linear line after some time. The elctrocatalyst, PB reacts to reduce H_2O_2 successfully, showing its excellent electrocatlaytic effects. The linearity is 0.9947 for rGO-PDDA-FePB with the sensitivity of 738.5 μA mM^{-1} cm^{-2} . From figure 22, the amperometric responses of rGO-PDDA-CuPB was shown. It was also done in 0.1M KCl and 10mM HCl with the applied potential of +0.17V. The linearity was 0.9991 and the sensitivity was 124.7 μA mM^{-1} cm^{-2}. From figure 23, the amperometric responses of rGO-PDDA-NiPB was exhibited. The applied potential was +0.17V. The sensitivity was given as 340.3 μA mM^{-1} cm-2 where the linearity correlation coeffiecient was 0.9974. Taking a look at table 1, the limit of detection for rGO-PDDA-FePB was 0.1μM, one for rGO-PDDA-CuPB was 0.57μM, rGO-PDDA-NiPB was 0.08μM. This comparison has given a clue that rGO-PDDA-NiPB has very low limit of detection. Comparing the sensitivities, the rGO-PDDA-FePB has the highest sensitivity values.

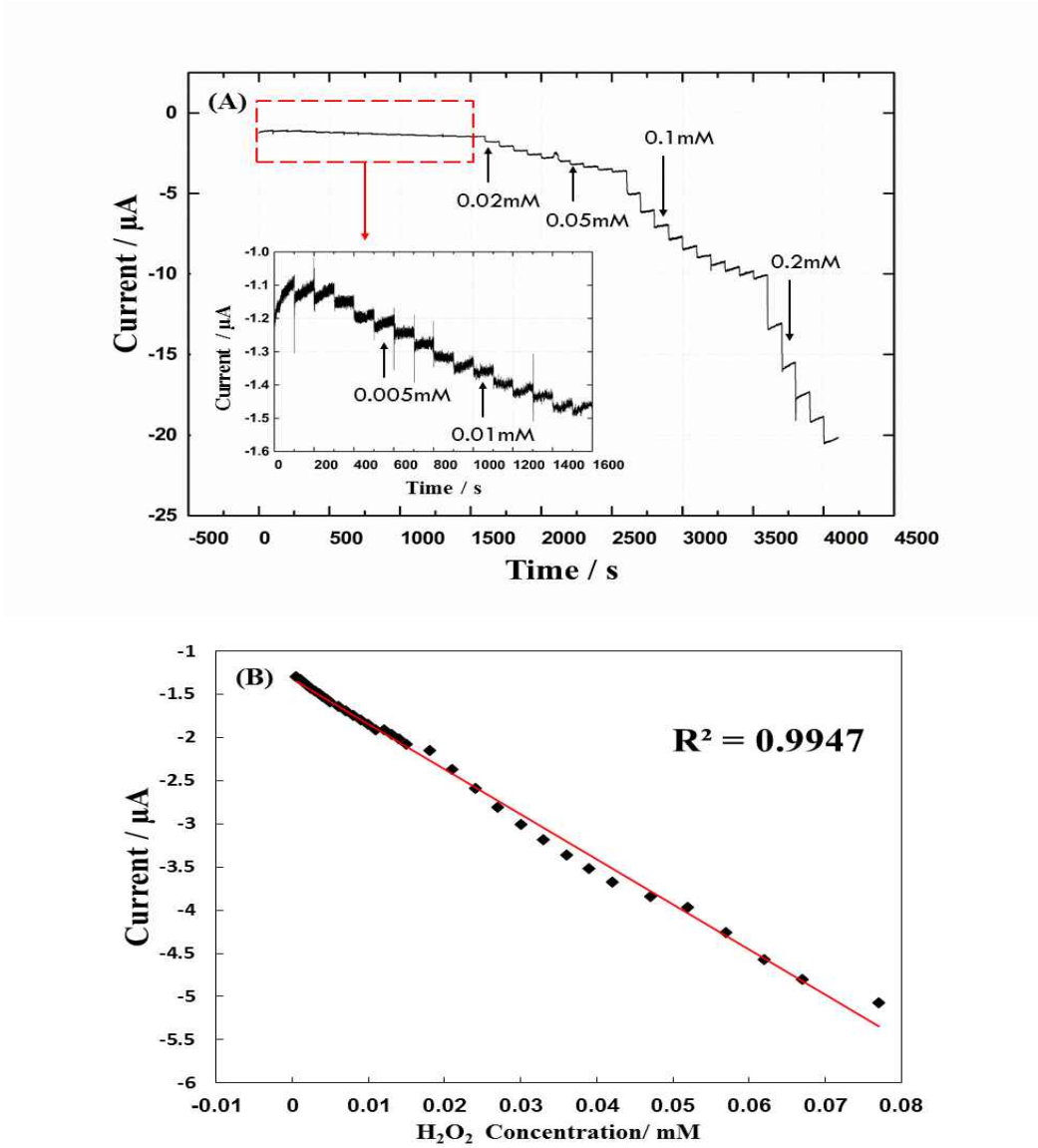

Figure 21. (A) Amperometric response of the rGO-PDDA-FePB nanocomposite modified glassy carbon electrode with injection of H_2O_2 in 0.1M KCl aqueous solution with 10mM HCl under stirring. The applied potential was +0.17V. (B) Calibration curve of the reduction peak current of rGO-PDDA-FePB modified electrode vs. H_2O_2 concentration

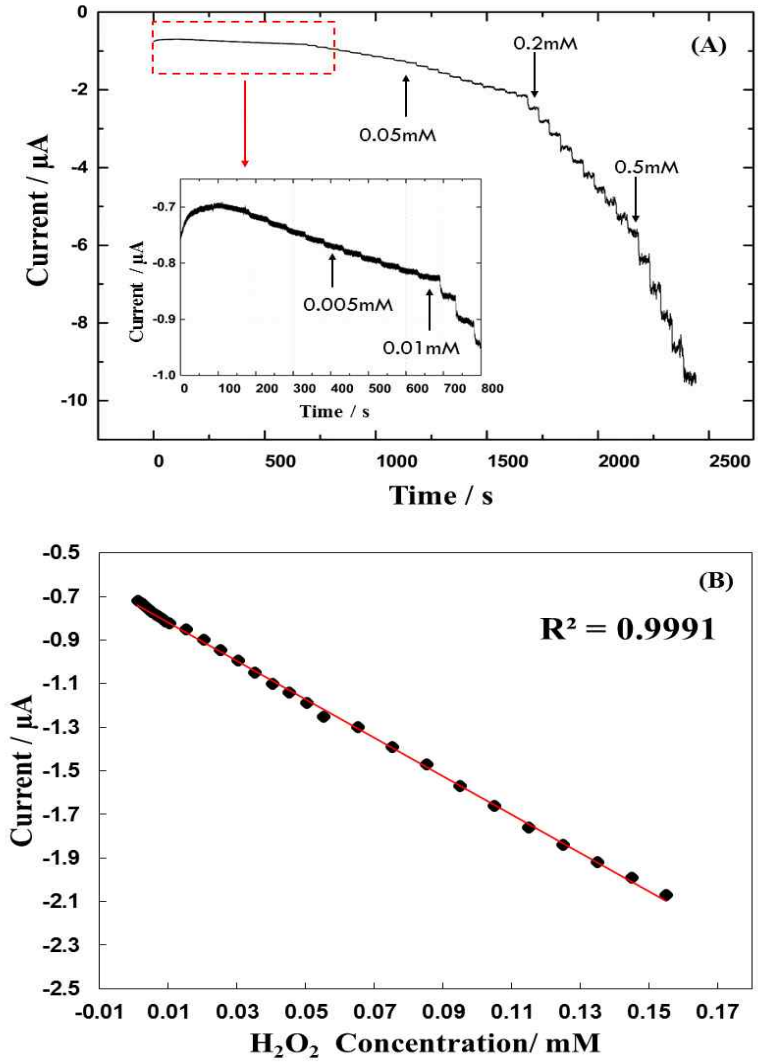

Figure 22. (A) Amperometric response of the rGO-PDDA-CuPB nanocomposite modified glassy carbon electrode with injection of H_2O_2 in 0.1M KCl aqueous solution with 10mM HCl under stirring. The applied potential was +0.17V. (B) Calibration curve of the reduction peak current of rGO-PDDA-CuPB modified electrode vs. H_2O_2 concentration

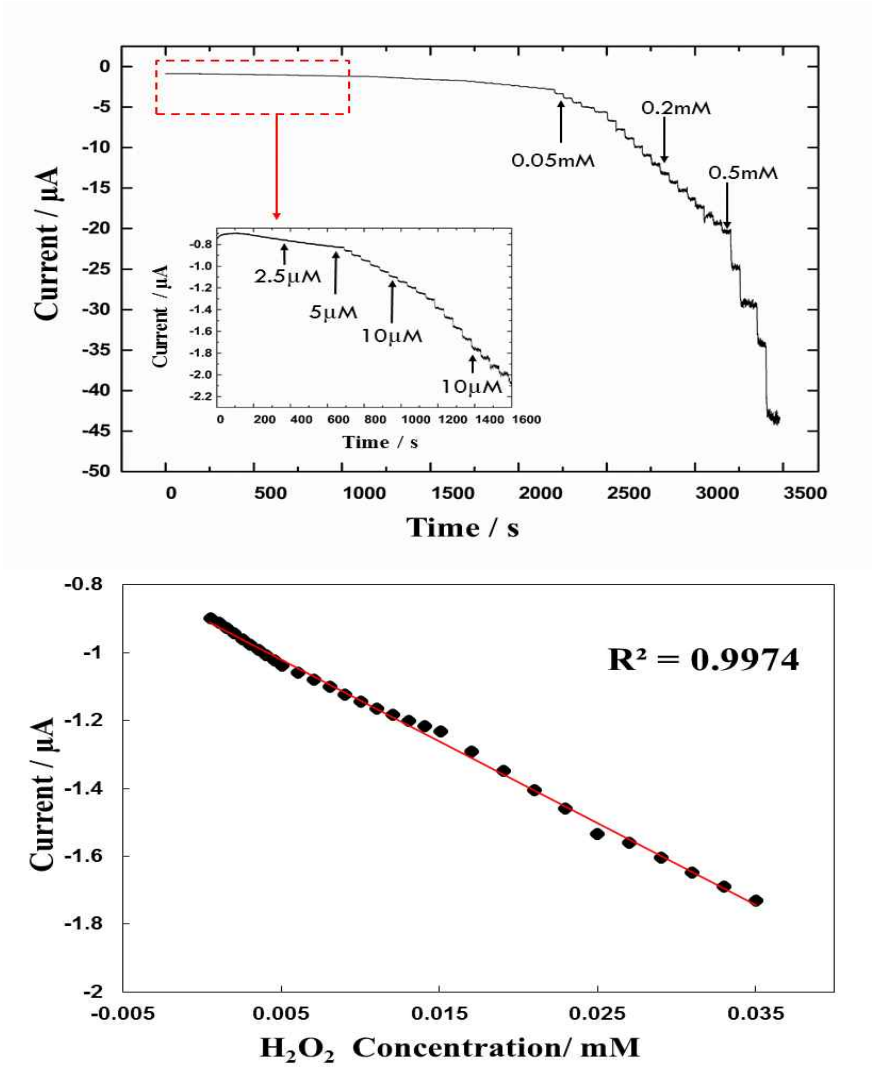

Figure 23. (A) Amperometric response of the rGO-PDDA-NiPB nanocomposite modified glassy carbon electrode with injection of H_2O_2 in 0.1M KCl aqueous solution with 10mM HCl under stirring. The applied potential was +0.17V. (B) Calibration curve of the reduction peak current of rGO-PDDA-NiPB modified electrode vs. H_2O_2 concentration

Electrode	Linear range (mM)	Sensitivity ($\mu A\ mM^{-1}\ cm^{-2}$)	Limit of detection (μM)	Applied Potential (V)	References
GCE/rGO-CNT/NiPB	0.0002-0.15	-	0.08	0.45	[75]
GCE/rGO/$Cu_2O_{(one\text{-}pot)}$	-	219.3	79.0	0.3	[76]
GCE/graphene/FePB	0.02-0.2	196.6	1.9	-0.05	[74]
GCE/rGO-PDDA-FePB	**0.0005–0.077**	**738.5**	**0.1**	**0.17**	**This work**
GCE/rGO-PDDA-CuPB	**0.001-0.155**	**124.7**	**0.57**	**0.17**	**This work**
GCE/rGO-PDDA-NiPB	**0.0005-0.035**	**340.3**	**0.08**	**0.17**	**This work**

Table 1. Electrochemical characteristics of various rGO-PB modified electrodes in determining hydrogen peroxide

4. Conclusion

In conclusion, the comparison of rGO-PDDA-FePB, rGO-PDDA-CuPB, and rGO-PDDA-NiPB has shown its possibility of sensitive electrochemical detection of H_2O_2. PDDA has definitely helped prussian blue analogues to be attached and well-defined onto rGO sheets. The studies of sensitivity of the amperometric responses of those materials has shown that a selective choice can be made according to appropriate applications. As each substance has its own characteristics, the further studies on its application should be considered. The high sensitivity and low limit of detection of those modified electrode is useful for the reduction of H_2O_2.

5. References

[1] S. Das, W. Choi, Graphene synthesis, Graphene: Synthesis and Applications; Series: Nanomaterials and their Applications CRC Press, October 2011.

[2] K.S. Novoselov , A.K. Geim, S.V. Morozov, D. Jiang, Y. Zhang, S.V. Dubonos, I.V. Grigorieva, A.A. Firsov, Electric field effect in atomically thin carbon films. Science. 306 (2004) 666–669.

[3] Sundaram R.S. Chemically derived graphene. In: Skákalová V., Schäffel F., Bachmatiuk A., Rümmeli M.H., editors. Graphene: properties, preparation, characterisation and devices. Sawston, Cambridge: Woodhead Publishing; 2014. p. 50–80. doi:10.1533/9780857099334.1.50

[4] Ibrahim I., Rümmeli M.H. Mechanical exfoliation. In: Warner J.H., Schäffel F., Bachmatiuk A., Rümmeli M.H., editors. Graphene: fundamentals and emergent applications. Kidlington, Oxford: Elsevier; 2013. p. 129–137.

[5] E. J-S. Amieva, J. López-Barroso, A. L. Martínez-Hernández, C. Velasco-Santos, Graphene Based Materials Functionalization with Natural Polymeric Biomolecules, Recent Advances in Graphene Research, Dr. Pramoda Nayak (Ed.), InTech. (2016)

[6] A.K. Geim, K. S. Novoselov, Nat. Mater. 2007, 6, 183.

[7] Bolotin, K. I., Sikes, K. J., Jiang, Z., Klima, M., Fudenberg, G., Hone, J., . . . Stormer, H. L. (2008). Ultrahigh electron mobility in suspended graphene. *Solid State Communications,*

146(9–10), 351-355.

[8] Morozov, S. V., Novoselov, K. S., Katsnelson, M. I., Schedin, F., Elias, D. C., Jaszczak, J. A., & Geim, A. K. (2008). Giant Intrinsic Carrier Mobilities in Graphene and Its Bilayer. *Physical Review Letters, 100*(1), 016602.

[9] Lee, C., Wei, X., Kysar, J. W., & Hone, J. (2008). Measurement of the Elastic Properties and Intrinsic Strength of Monolayer Graphene. *Science, 321*(5887), 385-388.

[10] Balandin, A. A., Ghosh, S., Bao, W., Calizo, I., Teweldebrhan, D., Miao, F., & Lau, C. N. (2008). Superior Thermal Conductivity of Single-Layer Graphene. *Nano Letters, 8*(3), 902-907.

[11] Cai, W., Zhu, Y., Li, X., Piner, R. D., & Ruoff, R. S. (2009). Large area few-layer graphene/graphite films as transparent thin conducting electrodes. *Applied Physics Letters, 95*(12), 123115.

[12] Li, X., Zhu, Y., Cai, W., Borysiak, M., Han, B., Chen, D., . . . Ruoff, R. S. (2009). Transfer of Large-Area Graphene Films for High-Performance Transparent Conductive Electrodes. *Nano Letters, 9*(12), 4359-4363.

[13] Zhu, Y., Murali, S., Cai, W., Li, X., Suk, J. W., Potts, J. R., & Ruoff, R. S. (2010). Graphene and Graphene Oxide: Synthesis, Properties, and Applications. *Advanced Materials, 22*(35), 3906-3924.

[14] Novoselov, K. S., Geim, A. K., Morozov, S. V., Jiang, D., Zhang, Y., Dubonos, S. V., . . . Firsov, A. A. (2004). Electric

Field Effect in Atomically Thin Carbon Films. *Science, 306*(5696), 666-669.

[15] Li, D., Muller, M. B., Gilje, S., Kaner, R. B., & Wallace, G. G. (2008). Processable aqueous dispersions of graphene nanosheets. *Nat Nanotechnol, 3*(2), 101-105.

[16] Lee, C., Wei, X., Kysar, J. W., & Hone, J. (2008). Measurement of the Elastic Properties and Intrinsic Strength of Monolayer Graphene. *Science, 321*(5887), 385-388.

[17] Kim, Y.-R., Bong, S., Kang, Y.-J., Yang, Y., Mahajan, R. K., Kim, J. S., & Kim, H. (2010). Electrochemical detection of dopamine in the presence of ascorbic acid using graphene modified electrodes. *Biosensors and Bioelectronics, 25*(10), 2366-2369.

[18] Liu, H., Xi, P., Xie, G., Shi, Y., Hou, F., Huang, L., . . . Wang, J. (2012). Simultaneous Reduction and Surface Functionalization of Graphene Oxide for Hydroxyapatite Mineralization. *The Journal of Physical Chemistry C, 116*(5), 3334-3341.

[19] Niyogi, S., Bekyarova, E., Itkis, M. E., McWilliams, J. L., Hamon, M. A., & Haddon, R. C. (2006). Solution Properties of Graphite and Graphene. *Journal of the American Chemical Society, 128*(24), 7720-7721.

[20] Liu, K., Zhang, J., Yang, G., Wang, C., & Zhu, J.-J. (2010). Direct electrochemistry and electrocatalysis of hemoglobin based on poly(diallyldimethylammonium chloride) functionalized graphene sheets/room temperature ionic liquid composite film.

Electrochemistry Communications, 12(3), 402-405.

[21] Zhang, D., Wang, K., Sun, D. C., Xia, X. H., & Chen, H. Y. (2003). Ultrathin Layers of Densely Packed Prussian Blue Nanoclusters Prepared from a Ferricyanide Solution. *Chemistry of Materials, 15*(22), 4163-4165.

[22] Zhang, D., Wang, K., Sun, D., Xia, X., & Chen, H. (2003). Potentiodynamic deposition of Prussian blue from a solution containing single component of ferricyanide and its mechanism investigation. *Journal of Solid State Electrochemistry, 7*(9), 561-566.

[23] Yang, C., Wang, C.-H., Wu, J.-S., & Xia, X. (2006). Mechanism investigation of Prussian blue electrochemically deposited from a solution containing single component of ferricyanide. *Electrochimica Acta, 51*(19), 4019-4023.

[24] Duncan, J. F., & Wigley, P. W. R. (1963). 206. The electronic structure of the iron atoms in complex iron cyanides. *Journal of the Chemical Society (Resumed)*(0), 1120-1125.

[25] Herren, F., Fischer, P., Ludi, A., & Haelg, W. (1980). Neutron diffraction study of Prussian Blue, $Fe_4[Fe(CN)_6]_3.xH_2O$. Location of water molecules and long-range magnetic order. *Inorganic Chemistry, 19*(4), 956-959.

[26] Itaya, K., Shoji, N., & Uchida, I. (1984). Catalysis of the reduction of molecular oxygen to water at Prussian blue modified electrodes. *Journal of the American Chemical Society, 106*(12), 3423-3429.

[27] Karyakin, A. A. (2001). Prussian Blue and its analogues: Electrochemistry and analytical applications. *Electroanalysis, 13*(10), 813-819.

[28] Kim, J., Kim, G., & Cremer, P. S. (2002). Investigations of Polyelectrolyte Adsorption at the Solid/Liquid Interface by Sum Frequency Spectroscopy: Evidence for Long-Range Macromolecular Alignment at Highly Charged Quartz/Water Interfaces. *Journal of the American Chemical Society, 124*(29), 8751-8756.

[29] Kim, J., & Cremer, P. S. (2000). IR−Visible SFG Investigations of Interfacial Water Structure upon Polyelectrolyte Adsorption at the Solid/Liquid Interface. *Journal of the American Chemical Society, 122*(49), 12371-12372.

[30] Jiang, S. P., Liu, Z., Tang, H. L., & Pan, M. (2006). Synthesis and characterization of PDDA-stabilized Pt nanoparticles for direct methanol fuel cells. *Electrochimica Acta, 51*(26), 5721-5730.

[31] Liu, F., Wang, L., Yin, Q., & Jiang, B. (2014). Optimization of thermoelectric figure of merit in poly(p-phenylenediamine)/exfoliated graphene nanosheets composites. *RSC Advances, 4*(93), 51558-51568.

[32] Liu, S.-Q., Xu, J.-J., & Chen, H.-Y. (2002). Electrochemical behavior of nanosized Prussian blue self-assembled on Au electrode surface. *Electrochemistry Communications, 4*(5), 421-425.

[33] Zhang, D., Zhang, K., Yao, Y. L., Xia, X. H., & Chen, H. Y.

(2004). Multilayer Assembly of Prussian Blue Nanoclusters and Enzyme-Immobilized Poly(toluidine blue) Films and Its Application in Glucose Biosensor Construction. *Langmuir, 20*(17), 7303-7307.

[34] Qiu, J.-D., Peng, H.-Z., Liang, R.-P., Li, J., & Xia, X.-H. (2007). Synthesis, Characterization, and Immobilization of Prussian Blue-Modified Au Nanoparticles: Application to Electrocatalytic Reduction of H_2O_2. *Langmuir, 23*(4), 2133-2137.

[35] Uemura, T., & Kitagawa, S. (2003). Prussian Blue Nanoparticles Protected by Poly(vinylpyrrolidone). *Journal of the American Chemical Society, 125*(26), 7814-7815.

[36] Zhang, X., Sui, C., Gong, J., Yang, R., Luo, Y., & Qu, L. (2007). Preparation, characterization, and property of polyaniline/Prussian blue micro-composites in a low-temperature hydrothermal process. *Applied Surface Science, 253*(22), 9030-9034.

[37] Sheng, Q., Zhang, D., Wu, Q., Zheng, J., & Tang, H. (2015). Electrodeposition of Prussian blue nanoparticles on polyaniline coated halloysite nanotubes for nonenzymatic hydrogen peroxide sensing. *Analytical Methods, 7*(16), 6896-6903.

[38] Husmann, S., Nossol, E., & Zarbin, A. J. G. (2014). Carbon nanotube/Prussian blue paste electrodes: Characterization and study of key parameters for application as sensors for determination of low concentration of hydrogen peroxide. *Sensors and Actuators B: Chemical, 192*, 782-790.

[39] Karyakin, A. A., Karyakina, E. E., & Gorton, L. (1998). The

electrocatalytic activity of Prussian blue in hydrogen peroxide reduction studied using a wall-jet electrode with continuous flow. *Journal of Electroanalytical Chemistry, 456*(1–2), 97-104.

[40] Kulesza, P. J., Miecznikowski, K., Malik, M. A., Galkowski, M., Chojak, M., Caban, K., & Wieckowski, A. (2001). Electrochemical preparation and characterization of hybrid films composed of Prussian blue type metal hexacyanoferrate and conducting polymer. *Electrochimica Acta, 46*(26–27), 4065-4073.

[41] Dong, S., & Che, G. (1991). Electrocatalytic oxidation of ascorbic acid at a prussian blue film modified microdisk electrode. *Journal of Electroanalytical Chemistry and Interfacial Electrochemistry, 315*(1), 191-199.

[42] Karyakin, A. A., Karyakina, E. E., & Gorton, L. (1999). On the mechanism of H_2O_2 reduction at Prussian Blue modified electrodes. *Electrochemistry Communications, 1*(2), 78-82.

[43] Zhou, J., & Wang, E. (1992). Sensitive amperometric detection of glucose by reversed phase liquid chromatography at a Prussian Blue chemically modified electrode of novel construct. *Journal of Electroanalytical Chemistry, 331*(1), 1029-1043.

[44] Neff, V.D., (1985). Some Performance Characteristics of a Prussian Blue Battery *J. Electrochem. Soc.* 132 (6) 1382-1384.

[45] Kaneko, M., & Okada, T. (1988). A secondary battery composed of multilayer Prussian Blue and its reaction characteristics. *Journal of Electroanalytical Chemistry and Interfacial Electrochemistry, 255*(1), 45-52.

[46] Deng, Z., & Smyrl, W. H. (1991). Application of Electroactive Films in Corrosion Protection: II . Metal Hexacyanometalate Films on Surfaces. *Journal of The Electrochemical Society, 138*(7), 1911-1918.

[47] Yu, Y., Chen, Z., He, S., Zhang, B., Li, X., & Yao, M. (2014). Direct electron transfer of glucose oxidase and biosensing for glucose based on PDDA-capped gold nanoparticle modified graphene/multi-walled carbon nanotubes electrode. *Biosensors and Bioelectronics, 52*, 147-152.

[48] Kulesza, P. J., Brajter, K., & Dabek-Zlotorzynska, E. (1987). Application of chelate-forming resin and modified glassy carbon electrode for selective determination of iron(III) by liquid chromatography with electrochemical detection. *Analytical Chemistry, 59*(23), 2776-2780.

[49] Cox, J. A., Jaworski, R., & Kulesza, P. J. (1991). Electroanalysis with electrodes modified by inorganic films. *Electroanalysis, 3*(9), 869-877.

[50] Humphrey, B. D., Sinha, S., & Bocarsly, A. B. (1984). Diffuse reflectance spectroelectrochemistry as a probe of the chemically derivatized electrode interface. Time-dependent diffussion. *The Journal of Physical Chemistry, 88*(4), 736-743.

[51] Coon, D. R., Amos, L. J., Bocarsly, A. B., & Fitzgerald Bocarsly, P. A. (1998). Analytical Applications of Cooperative Interactions Associated with Charge Transfer in Cyanometalate Electrodes: Analysis of Sodium and Potassium in Human Whole Blood. *Analytical Chemistry, 70*(15), 3137-3145.

[52] Koncki, R. (2002). Chemical Sensors and Biosensors Based on Prussian Blues. *Critical Reviews in Analytical Chemistry, 32*(1), 79-96.

[53] Kulesza, P. J., Brajter, K., & Dabek-Zlotorzynska, E. (1987). Application of chelate-forming resin and modified glassy carbon electrode for selective determination of iron(III) by liquid chromatography with electrochemical detection. *Analytical Chemistry, 59*(23), 2776-2780.

[54] Li, W., Yinjian, Y., Haozhi, Z., Yonghai, S., Shuijian, H., Fugang, X., & Haoqing, H. (2012). Controllable growth of Prussian blue nanostructures on carboxylic group-functionalized carbon nanofibers and its application for glucose biosensing. *Nanotechnology, 23*(45), 455502.

[55] Du, G., Lin, C., & Bocarsly, A. B. (1996). Electroanalytical Detection of Glucose Using a Cyanometalate-Modified Electrode: Requirements for the Oxidation of Buried Redox Sites in Glucose Oxidase. *Analytical Chemistry, 68*(5), 796-806.

[56] Zamponi, S., Berrettoni, M., Kulesza, P. J., Miecznikowski, K., Malik, M. A., Makowski, O., & Marassi, R. (2003). Influence of experimental conditions on electrochemical behavior of Prussian blue type nickel hexacyanoferrate film. *Electrochimica Acta, 48*(28), 4261-4269.

[57] Tani, Y., Eun, H., & Umezawa, Y. (1998). A cation selective electrode based on copper(II) and nickel(II) hexacyanoferrates: dual response mechanisms, selective uptake or adsorption of analyte cations. *Electrochimica Acta, 43*(23), 3431-3441.

[58] Wang, J., Zhang, X., & Prakash, M. (1999). Glucose microsensors based on carbon paste enzyme electrodes modified with cupric hexacyanoferrate. *Analytica Chimica Acta, 395*(1–2), 11-16.

[59] de Mattos, I. L., Gorton, L., Laurell, T., Malinauskas, A., & Karyakin, A. A. (2000). Development of biosensors based on hexacyanoferrates. *Talanta, 52*(5), 791-799.

[60] Narayanan, S. S., & Scholz, F. (1999). A comparative study of the electrocatalytic activities of some metal hexacyanoferrates for the oxidation of hydrazine. *Electroanalysis, 11*(7), 465-469.

[61] Garjonyte, R., & Malinauskas, A. (1999). Operational stability of amperometric hydrogen peroxide sensors, based on ferrous and copper hexacyanoferrates. *Sensors and Actuators B-Chemical, 56*(1-2), 93-97.

[62] Malik, M. A., & Kulesza, P. J. (1996). Preparation and characterization of Ag-intercalated copper hexacyanoferrate films on electrodes. *Electroanalysis, 8*(2), 113-116.

[63] Chen, S., Yuan, R., Chai, Y., & Hu, F. (2013). Electrochemical sensing of hydrogen peroxide using metal nanoparticles: a review. *Microchimica Acta, 180*(1), 15-32.

[64] Sitnikova, N. A., Borisova, A. V., Komkova, M. A., & Karyakin, A. A. (2011). Superstable Advanced Hydrogen Peroxide Transducer Based on Transition Metal Hexacyanoferrates. *Analytical Chemistry, 83*(6), 2359-2363.

[65] Li, Y.-z., & Townshend, A. (1998). Evaluation of the adsorptive

immobilisation of horseradish peroxidase on PTFE tubing in flow systems for hydrogen peroxide determination using fluorescence detection. *Analytica Chimica Acta, 359*(1–2), 149-156.

[66] Hanaoka, S., Lin, J.-M., & Yamada, M. (2001). Chemiluminescent flow sensor for H_2O_2 based on the decomposition of H_2O_2 catalyzed by cobalt(II)-ethanolamine complex immobilized on resin. *Analytica Chimica Acta, 426*(1), 57-64.

[67] Cinti, S., Arduini, F., Moscone, D., Palleschi, G., & Killard, A. (2014). Development of a Hydrogen Peroxide Sensor Based on Screen-Printed Electrodes Modified with Inkjet-Printed Prussian Blue Nanoparticles. *Sensors, 14* (8), 14222.

[68] Tian, Z. Q., Jiang, S. P., Liu, Z., & Li, L. (2007). Polyelectrolyte-stabilized Pt nanoparticles as new electrocatalysts for low temperature fuel cells. *Electrochemistry Communications, 9*(7), 1613-1618.

[69] Zhu, Y., Stoller, M. D., Cai, W., Velamakanni, A., Piner, R. D., Chen, D., & Ruoff, R. S. (2010). Exfoliation of Graphite Oxide in Propylene Carbonate and Thermal Reduction of the Resulting Graphene Oxide Platelets. *ACS Nano, 4*(2), 1227-1233.

[70] Shin, H.-J., Kim, K. K., Benayad, A., Yoon, S.-M., Park, H. K., Jung, I.-S., . . . Lee, Y. H. (2009). Efficient Reduction of Graphite Oxide by Sodium Borohydride and Its Effect on Electrical Conductance. *Advanced Functional Materials, 19*(12),

1987-1992.

[71] Cote, L. J., Cruz-Silva, R., & Huang, J. (2009). Flash Reduction and Patterning of Graphite Oxide and Its Polymer Composite. *Journal of the American Chemical Society, 131*(31), 11027-11032.

[72] Vaucher, S., Li, M., & Mann, S. (2000). Synthesis of prussian blue nanoparticles and nanocrystal superlattices in reverse microemulsions. *Angewandte Chemie International Edition, 39*, 1793-1796.

[73] Garjonyt≐, R., & Malinauskas, A. (1998). Electrocatalytic reactions of hydrogen peroxide at carbon paste electrodes modified by some metal hexacyanoferrates. *Sensors and Actuators B: Chemical, 46*(3), 236-241.

[74] Xu, C., Wang, X., & Zhu, J. (2008). Graphene−Metal Particle Nanocomposites. *The Journal of Physical Chemistry C, 112*(50), 19841-19845.

[75] Deng, K., Li, C., Qiu, X., Zhou, J., & Hou, Z. (2015). Electrochemical preparation, characterization and application of electrodes modified with nickel–cobalt hexacyanoferrate/graphene oxide–carbon nanotubes. *Journal of Electroanalytical Chemistry, 755*, 197-202.

[76] Xu, F., Deng, M., Li, G., Chen, S., & Wang, L. (2013). Electrochemical behavior of cuprous oxide–reduced graphene oxide nanocomposites and their application in nonenzymatic hydrogen peroxide sensing. *Electrochimica Acta, 88*, 59-65.

[77] Ding, Y., Gu, G., & Xia, X.-H. (2008). Electrochemical deposition and mechanism investigation of Prussian blue on graphic carbon paste electrode from an acidic ferricyanide solution. *Journal of Solid State Electrochemistry, 12*(5), 553-558.

국문 요약

환원 그래핀 옥사이드-폴리(디알릴디메틸암모늄 클로라이드)과 니켈, 철, 구리 프러시안 블루의 합성과 과산화수소의 검출 비교 연구

본 연구는 환원 그래핀 옥사이드 (reduced graphene oxide, rGO) - 폴리(디알릴디메틸암모늄 클로라이드) (poly(diallyldimethylammonidum chloride, PDDA)-프러시안 블루 (Prussian blue, PB) 나노복합물을 합성하는 방법을 제시하고, 그에 따른 과산화수소 검출을 연구하였다. 먼저 환원 그래핀 옥사이드와 폴리(디알릴디메틸암모늄 클로라이드)와 수산화 붕소 나트륨을 사용하여, 환원 그래핀 옥사이드-폴리(디알릴디메틸암모늄 클로라이드)를 합성한 후, 전극(glassy carbon electrode, GCE)에 합성된 물질의 용액형태로 올린 후 건조하였다. 개질된 전극에 니켈, 철 구리 프러시안 블루를 전해석출방법 (electrodeposition)을 사용하여 전착하도록 하였다.

푸리에 변환 적외분광법 (Fourier transform infrared spectroscopy, FT-IR)과 주사형 전자 현미경 사진 (scanning electron micrograph,

SEM)을 주로 사용하여 구조와 화학적 구성을 연구하였다.
니켈, 철, 구리 프러시안 블루와 환원 그래핀 옥사이드-폴리(디알릴디메틸암모튬 클로라이드) 개질 전극을 이용하여 연구를 진행하였다. 불안정한 그래핀 옥사이드에 폴리(디알릴디메틸암모늄 클로라이드)는 프러시안 블루가 잘 형성되도록 도우며, 프러시안 블루가 과산화수소 측정 및 검출에 대한 시너지 효과를 높이며 촉매능력을 하도록 도와줌을 확인할 수 있었다.
본 연구에서는 10mM 염산과 0.1M 염화칼륨인 용액을 기본 수용액으로 사용하여 순환전류법(CV)와 시간전류법 (Amperometry)의 분석방법으로 분석을 하였으며, 산성 용액에서 전기화학적 촉매역할을 하는 것을 보였다. 특히 니켈, 철, 구리 프러시안 블루가 환원 그래핀 옥사이드-폴리(디알릴디메틸암모늄 클로라이드)에 개질되었을 때 나타나는 현상을 비교함으로서 철 프러시안 블루의 높은 감도 (738.5 μA mM^{-1} cm^{-2})은 과산화수소의 전기화학적 검출에 철 프러시안 블루가 감도가 높으며, 낮은 검출한계를 보여준 rGO-PDDA-NiPB는 비록 높은 과산화수소 농도에는 높은 감도를 보이지 않지만, 낮은 검출한계를 보이고 있어 선택적으로 사용할 수 있을 것으로 기대한다.

주요어: 철 프러시안 블루, 니켈 프러시안 블루, 구리 프러시안 블루, 과산화수소, 환원 그래핀 옥사이드, 폴리(디알릴디메틸암모늄 클로라이드)

***Student Number* : 2014-22855**